

1 **Acidification, warming, and nutrient management are projected to**
2 **cause reductions in shell and tissue weights of oysters in a coastal plain**
3 **estuary**

4 Catherine R. Czajka¹, Marjorie A.M. Friedrichs¹, Emily B. Rivest¹, Pierre St-Laurent¹, Mark J. Brush¹,
5 and Fei Da²

6 ¹Virginia Institute of Marine Science, William & Mary, Gloucester Point, VA, 23062, USA

7 ²Department of Geosciences, Princeton University, Princeton, NJ, 08544, USA

8 *Correspondence to:* Catherine R. Czajka (czajkacatherine@gmail.com)

9 **Abstract.** Coastal acidification, warming, and nutrient management actions all alter water quality conditions that marine
10 species experience, with potential impacts to their physiological processes. Decreases in calcite saturation state (Ω_{Ca}) and food
11 availability, combined with warming water temperatures, pose a threat to calcifying organisms; however, the magnitude of
12 future changes in estuarine systems is challenging to predict and is not well known. This study aims to determine how and
13 where oysters will be affected by future acidification, warming, and nutrient reductions, and the relative effects of these
14 stressors. To address these goals, an oyster bioenergetics model for Eastern oysters (*Crassostrea virginica*) was embedded in
15 a 3-D coupled hydrodynamic-biogeochemistry model implemented for two tributaries in the lower Chesapeake Bay. Model
16 simulations were forced with projected future conditions (mid-21st century atmospheric CO₂, and atmospheric temperature,
17 under representative concentration pathway (RCP) 8.5, as well as managed nutrient reductions) and compared with a realistic
18 present-day reference run. Together, all three stressors are projected to reduce Ω_{Ca} and growth of oyster shell and tissue.
19 Increased atmospheric CO₂ and temperature are both projected to cause widespread reductions in Ω_{Ca} . The resulting reductions
20 in oyster shell and tissue growth will be most severe along the tributary shoals. Future warming during peak oyster growing
21 seasons is projected to have the strongest negative influence on tissue and shell growth, due to summer water temperatures
22 reducing filtration rates, enhancing shell dissolution and oyster respiration rates, and increasing organic matter remineralization
23 rates, thus reducing food availability. Nutrient reductions will exacerbate deficits in oyster food availability, contributing to
24 further reductions in growth. Quantifying the effects of these stressors provides insight on the areas in the lower bay where
25 oysters will be most vulnerable to mid 21st-century conditions.

26
27 **Short summary.** Under future acidification, warming, and nutrient management, substantial reductions in shell and tissue
28 weights of Eastern oysters are projected for the Chesapeake Bay. Lower oyster growth rates will be largely driven by reduced
29 calcium carbonate saturation states and reduced food availability. Oyster aquaculture practices in the region will likely be
30 affected, with site selection becoming increasingly important as impacts will be highly spatially variable.

Style Definition: Default Paragraph Font

Formatted: Tab stops: Not at 4.13"

Deleted: ,

Deleted: , and

33 **1 Introduction**

34 Anthropogenic climate change and its associated impacts on water quality may threaten marine organisms and
35 economic systems reliant on them. Oceanic uptake of increasing anthropogenic atmospheric carbon dioxide (CO₂) causes a
36 decrease in seawater pH and saturation states of calcium carbonate (e.g., Ω_{Ca}), a phenomenon known as ocean acidification
37 (Caldeira and Wickett, 2003; Doney et al., 2009). Globally, the ocean has absorbed about 30% of anthropogenic atmospheric
38 CO₂ since pre-industrial times (Gruber et al., 2019), and open-ocean surface pH is anticipated to decrease by 0.3 units on
39 average relative to the 2010s by the end of the century under ‘business-as-usual’ conditions (Riahi et al., 2011; IPCC, 2019).
40 The percent volume of ocean water undersaturated with calcite ($\Omega_{Ca} < 1$), a condition associated with elevated energetic costs
41 of shell-building for calcifying organisms, is predicted to expand to 91% by 2100 from 76% in the 1990s (Caldeira and Wickett,
42 2005; Gattuso et al., 2015). Concurrently, the global ocean has absorbed approximately 93% of the atmospheric heat produced
43 by anthropogenic activity, leading to a global sea surface temperature increase of 0.7°C since 1900 (Jewett and Romanou,
44 2017). Ocean warming is expected to continue, with global averages increasing by 2.7°C by 2100 and greater increases
45 expected in shallow coastal regions (Jewett and Romanou, 2017).

46 Since estuaries have lower and more variable pH than the open-ocean, the effects of increased CO₂ and warming on
47 estuarine water quality and biota are often amplified. In coastal and estuarine systems, acidification may be exacerbated by
48 local-level processes, such as the input of acidic freshwater and nutrient runoff from precipitation, a process termed coastal
49 acidification (Salisbury et al., 2008; Wallace et al., 2014; Carstensen and Duarte, 2019). Coastal acidification may accelerate
50 as warming of coastal waters increases rates of biogeochemical processes; increased respiration rates may drive larger diel
51 variations in pH, dissolved oxygen, and associated water quality (Du et al., 2018; Tian et al., 2021). Freshwater has relatively
52 low total alkalinity (TA), or buffering capacity, so estuarine areas with greater relative freshwater influence cannot resist
53 changes to pH as easily as more saline or open-ocean waters (Hasler et al., 2018; Pacella et al., 2024). Eutrophication, the
54 increased rate of organic matter input to a system (Nixon, 1995), may also drive large variations in local pH and overall water
55 quality. Elevated nutrient inputs cause pH to increase in surface waters due to higher primary productivity, which will reduce
56 surface acidification; however, pH will decrease in deeper bottom waters as the additional organic matter sinks and is
57 remineralized (Cai et al., 2021). Management actions to reduce eutrophication and improve water quality in bottom waters
58 have been successful but may also enhance acidification in shallow surface waters by lowering primary productivity (Borges
59 and Gypens, 2010; Da et al., 2021). The overall effect of future changes in nutrient inputs on coastal biogeochemistry is thus
60 unclear, particularly in the presence of warming and acidification.

61 Characterizing spatiotemporal patterns of acidification in estuarine waters is important, as negative impacts of
62 acidification on the biology of marine organisms may be substantial. Acidification disrupts the formation of calcium carbonate
63 (CaCO₃) during shell-building, i.e., biocalcification, which is a vital process for growth and survival of many aquatic
64 invertebrate species (e.g., Orr et al., 2005; Gazeau et al., 2007; Dong et al., 2023). Under acidified conditions, water
65 concentrations of CO₂ and H⁺ increase, and concentrations of carbonate ions ([CO₃²⁻]) decrease. A low ambient [CO₃²⁻] inhibits

Formatted: Font: Not Bold

Deleted: ,

Formatted: Font: Not Bold

Deleted:)

Formatted: Font: Not Bold

Moved down [1]: In coastal and estuarine systems, acidification may be exacerbated by local-level processes, such as the input of acidic freshwater and nutrient runoff from precipitation, a process termed coastal acidification (Salisbury et al., 2008; Wallace et al., 2014; Carstensen and Duarte, 2019).

Moved down [2]: Elevated nutrient inputs cause pH to increase in surface waters due to higher primary productivity, which will reduce surface acidification; however, pH will decrease in deeper bottom waters as the additional organic matter sinks and is remineralized (Cai et al., 2021). Management actions to reduce eutrophication and improve water quality in bottom waters have been successful but may also enhance acidification in shallow surface waters by lowering primary productivity (Borges and Gypens, 2010). The overall effect of future changes in nutrient

Deleted: ¶

Since estuaries have lower and more variable pH than the open-ocean, the effects of increased CO₂ on estuarine water quality and biota are often amplified.

Deleted: Freshwater has relatively low total alkalinity (TA), or buffering capacity, so areas in estuaries with greater relative freshwater influence cannot resist changes to pH as easily as more saline or open-ocean waters (Hasler et al., 2018; Pacella et al., 2024). Eutrophication, the increased rate of organic matter input to a system (Nixon, 1995), may drive large variations in local pH and overall water quality.

Deleted:). The overall effect of future changes in nutrient inputs on coastal biogeochemistry is thus unclear. ¶ (... [1])

Formatted: Font: Not Bold

Formatted: Font: Not Bold

Formatted: Font: Not Bold

Formatted: Heading 1, Line spacing: 1.5 lines

Moved (insertion) [1]

Formatted: Font: Not Bold

Deleted: Therefore, it is vital to understand how warm (... [2])

Deleted: acidification to predict local

Formatted: Font: Not Bold

Formatted: Font: Not Bold

Formatted: Font: Not Bold

Moved (insertion) [2]

Formatted: Font: Not Bold

Deleted: water quality and health of coastal organisms

Formatted: Font: Not Bold

105 calcifying organisms from forming CaCO_3 for their shells, as more energy is required to precipitate CO_3^{2-} from acidified waters
106 (e.g., Guinotte and Fabry, 2008; Lutier et al., 2022; Matoo et al., 2020; Mederios and Souza, 2023). Low Ω_{Ca} may also lead to
107 net dissolution of CaCO_3 , leading to weaker shells and greater juvenile susceptibility to predation (e.g., Waldbusser et al.,
108 2011; Amaral et al., 2012; Barclay et al., 2020). Acidification may further reduce shell growth through adverse physiological
109 effects that limit energy availability for calcification. Because acidification is often more extreme in estuaries, coastal bivalve
110 species experience stronger effects of climate change than organisms living in open-ocean environments (Poach et al., 2019;
111 Melzner et al., 2020; Cai et al., 2021). **Oysters in particular are of high management and research interest due to their**
112 **commercial value in the United States (USDA, 2023).** Prior experiments have revealed negative effects of acidification,
113 warming, and nutrient reductions on oyster biocalcification and growth (Beniash et al., 2010; Waldbusser et al., 2011; Gobler
114 and Talmage, 2014), but it is yet to be determined how the impacts of these stressors on oyster shell and tissue growth will
115 vary spatially in highly dynamic systems.

116 The Chesapeake Bay is an excellent study system for examining the interacting influences of acidification, warming,
117 and nutrient reductions (hereafter referred to collectively as “future stressors”) on estuarine biogeochemistry and the organisms
118 living there. The bay exhibits high temporal and spatial variability in pH due to seasonal phytoplankton blooms, eutrophication,
119 and acidic freshwater input (Da et al., 2021; St-Laurent et al., 2020; Kemp et al., 2005; Cai et al., 2021). From the mid-1980s
120 to mid-2010s, surface waters in the upper bay experienced pH increases between +0.2 and +0.4 pH units in early spring and
121 fall due to increased riverine TA from reduced acid mine drainage and lowered nitrate inputs, while surface waters in the
122 nitrogen-limited middle bay decreased up to -0.24 pH units during late spring and summer as a result of decreased primary
123 production (Da et al., 2021). Over the same time period, the bay warmed by $0.24 \pm 0.15^\circ\text{C}$ per decade (Hinson et al., 2022),
124 more than double the average rate of warming for the upper 75m of the global ocean (Rhein et al., 2013). Warming has also
125 led to more severe hypoxia (Irby et al., 2018; Ni et al., 2020; Frankel et al., 2022; Hinson et al., 2023; **Hinson et al., 2024**). In
126 2010, the Environmental Protection Agency mandated a Total Maximum Daily Load (TMDL) of pollutants from point and
127 non-point sources to be achieved by 2025 (EPA, 2010). As nutrient reductions negatively affect pH in surface waters of the
128 bay (Shen et al., 2020; Da et al., 2021), achieving the TMDLs may actually worsen acidification in shallow and near-shore
129 regions. Much of the research effort devoted to characterizing present-day carbonate chemistry and its historical trends has
130 focused on the mainstem and upper Chesapeake Bay (Cai et al., 2017; Shen et al., 2020; Su et al., 2020), and less is known
131 about these conditions throughout the tributaries of the lower bay (Shadwick et al., 2019).

132 The combined effects of future stressors will impact calcifying organisms in the lower Chesapeake Bay as well as the
133 economic systems reliant upon them. The Eastern oyster *Crassostrea virginica* (Gmelin, 1791) is a foundation species native
134 to the bay (Dayton, 1972). Eastern oyster aquaculture in this region has grown rapidly in the past few decades, with Virginia
135 becoming the third most productive oyster fishery in 2018 (Hudson, 2019), largely a result of the development of disease-
136 resistant oyster strains (Frank-Lawale et al., 2014). Negative impacts of acidification on aquaculture practices in other parts of
137 the world (Barton et al., 2015) have already stirred concern over the vulnerability of oysters in the Chesapeake Bay. For
138 example, in the Pacific Northwest, major larval mortality occurred at a shellfish hatchery following an upwelling event that

Deleted: oysters and other commercially valuable

Deleted: 2021;).

Formatted: Font: Bold

Deleted:).

lowered pH and Ω of aragonite, which had cascading impacts on the oyster industry all along the West Coast (Barton et al., 2015). While most effects of acidification on aquaculture have been observed in oyster larvae in hatcheries, fewer studies have examined acidification's influence on adult oysters when deployed in the field. Water quality conditions within oyster farms can be highly spatially variable, so the impacts of acidification may vary with growing conditions (Saavedra et al., 2024; Simpson et al., 2024). To support the future of the oyster aquaculture industry in Chesapeake Bay, it is critical to identify which areas in the bay will be most vulnerable to acidification at mid-century and how each driver of change contributes to acidification and its impacts on growth.

This study addresses the following primary research question: How and where will carbonate chemistry and Eastern oyster growth in the lower Chesapeake Bay change in the future and which future stressors will drive these changes? A three-dimensional hydrodynamic-biogeochemical model is coupled with an oyster bioenergetics model and is applied to two major Virginia tributaries of the Chesapeake Bay. The model provides detailed information on present-day environmental conditions, and when combined with climate projections from Earth System Models, allows for simulations of the independent and interacting influences of future environmental change on carbonate chemistry and Eastern oysters. This study provides insight into which areas are most vulnerable to mid 21st-century acidification and how acidification, warming, and nutrient loading may each impact oyster growth in isolation as well as via simultaneous co-stressors.

2 Methods

2.1 Model description

2.1.1 Hydrodynamic model

This study uses the three-dimensional hydrodynamic Regional Ocean Modeling System (ROMS; Shchepetkin and McWilliams, 2005), implemented similarly to St-Laurent and Friedrichs (2024) but on a higher resolution grid focused on two of the lower Virginia Chesapeake Bay tributaries (Fig. 1). The model domain (Da et al., 2024) includes the York and Rappahannock Rivers, as well as a portion of the mainstem shoal north of the Rappahannock. The model grid consists of 620x740 horizontal grid cells with a horizontal resolution of 120 m, allowing for greater resolution of coastlines than many other Chesapeake Bay model grids (Irby et al., 2016). The hydrodynamic model includes 20 terrain-following vertical levels and two primary state variables: practical salinity and potential temperature. A wetting and drying scheme has been implemented to represent water levels and currents in coastal grid cells (Warner et al., 2013; St-Laurent and Friedrichs, 2024).

2.1.2 Carbon and biogeochemistry model

The Estuarine-Carbon-Biogeochemistry model (ECB) embedded in ROMS and used in this study has previously been implemented in the Chesapeake Bay (Feng et al., 2015; St-Laurent et al., 2020; Frankel et al., 2022; Hinson et al., 2023) as well as in the lower Virginia tributaries (Da et al., 2024). ECB simulates full carbon and nitrogen cycles of the lower trophic

172 levels, represented by the following state variables: nitrate, ammonium, phytoplankton and zooplankton nitrogen, small and
173 large detrital nitrogen and carbon, semi-labile and refractory dissolved organic nitrogen, DIC, TA, and dissolved oxygen (O₂).
174 Phytoplankton and zooplankton carbon are calculated from fixed C:N ratios (Redfield, 1934; Hopkinson et al., 1998). C:N
175 ratios for dissolved organic matter in the estuary are allowed to freely evolve with time. Biogeochemical processes include
176 primary production, aggregation, sinking, basal metabolism, exudation, sloppy feeding, excretion, metabolism,
177 nitrification/denitrification, remineralization, grazing, and mortality. Biogeochemical sources and sinks are included in the
178 bottom vertical level (e.g., burial, resuspension, nitrification/denitrification, remineralization, sediment O₂ and CO₂ exchange).
179 Light attenuation throughout the water column is based on the diffuse attenuation coefficient (K_d), which is parameterized as
180 a function of surface total suspended solids (TSS; including inorganic and organic components) and salinity as a proxy for
181 colored dissolved organic matter (Feng et al., 2015; Turner et al., 2021). TSS is calculated within the model as the sum of the
182 four inorganic suspended sediment size classes and particulate organic matter. Particulate organic carbon (POC) is calculated
183 as the sum of phytoplankton carbon, zooplankton carbon, and small and large detrital carbon. The sediment transport module
184 within ECB accounts for sediment-water exchange processes, such as deposition and resuspension of inorganic sediment and
185 particulate organic matter, and is comprised of two vertical seabed layers that simulate four suspended sediment size classes
186 (Turner et al., 2021).

187 The inorganic carbon module within ECB has been fine-tuned in this implementation of the model, allowing for
188 improved performance in carbonate system simulations (Da et al., 2024). The model grid includes tidal wetlands along the
189 York River based on estimated wetland areas (Mitchell et al., 2017), which further contribute to TA fluxes through sulfate
190 reduction in sediments (Raymond et al., 2000; Najjar et al., 2020). Ω_{Ca} is calculated from DIC, TA, temperature, and salinity
191 using CO2SYS (van Heuven et al., 2011) using the equilibrium constants of Cai and Wang (1998) as they are suitable for both
192 fresh and estuarine waters (Dinauer and Mucci, 2017; Herrmann et al., 2020). Although submerged aquatic vegetation is a
193 possible source of CaCO₃ (Mazarrasa et al., 2015; Su et al., 2020), CaCO₃ precipitation and dissolution are not simulated in
194 ECB due to both insufficient observations and low submerged aquatic vegetation presence throughout the model domain (Orth
195 et al., 1998; Moore et al., 2009).

196 Several additional updates have been made in this implementation of ROMS-ECB to better represent oxygen and
197 primary production dynamics in the lower Virginia tributaries. The maximum phytoplankton growth rate has been increased
198 to 2.15 d⁻¹, and the growth rate is limited in the fresh portion of the tributaries using a Michaelis-Menten function of salinity
199 and a half-saturation of 1.5 (Da et al., 2024). The sediment bed climatology from Moriarty et al. (2021) has been adjusted to
200 better represent the sand class distributions published in Nichols (1991) and observations taken by the USGS (Reid et al.,
201 2005). Specifically, the changes include a greater percentage of small clay-rich flocs throughout the main stem of the York
202 River as well as more sand and large silt-rich flocs in the Rappahannock River. Previously, the sediment module assumed the
203 same critical shear stress for large silt-rich flocs, small clay-rich flocs, and unaggregated mud; here, the critical shear stress of
204 smaller particles is lower than larger particles, meaning smaller particles resuspend more easily. The updated critical shear
205 stress coefficient for erosion and deposition is 0.5 Pa for large silt-rich flocs and 0.4 Pa for both small clay-rich flocs and

Deleted: and dissolved organic carbon (DOC)

Deleted: established

Deleted: Additional biogeochemical

Deleted: The sediment transport module within ECB

Deleted: greater

Deleted: minimum

unaggregated mud, which represent a small portion of the sediment bed. The ballasting formulation of Turner et al. (2021) has also been added to simulate the increase in particle sinking rates due to the aggregation of particles in turbid waters.

2.1.3 Oyster bioenergetics model

As part of this study, the oyster bioenergetics model EcoOyster (Brush and Kellogg, 2018; Kellogg et al., 2018) has been one-way coupled to ROMS-ECB in the deepest (bottom) level (see Supplementary Tables S1-S4 for EcoOyster equations). The one-way coupling means that environmental conditions from ROMS-ECB influence oyster growth in EcoOyster, but the oysters do not influence water quality conditions in ROMS-ECB. This allows the focus of our analysis to be on the effect of future climate change on oyster growth, rather than the effect of oyster growth on water quality, which has been previously studied in the Chesapeake Bay (e.g., Gawde et al., 2024). By focusing on the deepest vertical level of the model, the assumption is that oysters are growing on the bottom, and not inside floating cages. This is representative of conditions similar to on-bottom or bottom cage aquaculture methods that are common in Virginia. The coupled model, referred to hereafter as ROMS-ECBO, simulates daily somatic tissue dry weight, gonadal tissue dry weight, shell dry weight, and shell height of diploid and triploid oysters as a function of filtration, respiration, egestion, allocation to reproduction, calcification, and dissolution (Brush and Kellogg, 2018; Kellogg et al., 2018; Rivest et al., 2023). For the purpose of this study, only diploid oysters were included, as model equations were developed from a study on diploid oysters, and triploid allometric equations are not as well constrained. Tissue growth rates depend on individual weight together with temperature, salinity, O₂, TSS, and POC from ROMS-ECB. Chl_a is required for the filtration function and is calculated from ROMS-ECB phytoplankton carbon and K_d, in combination with seasonal carbon:chl_a ratios that are computed using equations from Cerco and Noel (2004). The calcification function includes a threshold value of $\Omega_{Ca} = 0.93$, determined through laboratory experiments with Eastern oysters (Rivest et al., 2023).

The EcoOyster equations were developed from a meta-analysis of existing oyster bioenergetics models and laboratory experiments with diploid oysters (Brush and Kellogg, 2018; Kellogg et al., 2018; Rivest et al., 2023). Allometric relationships between shell dry weight, tissue dry weight, and shell height used for initial conditions were derived from observational data in the Chesapeake Bay (VOSARA, 2024). Total dry tissue weight is calculated as the sum of somatic tissue weight and gonadal weight. Reproduction is simulated through gonadal weight, a function of growth of gonadal tissue, resorption of gonadal tissue, and spawning (Hofmann et al., 1994). Somatic tissue weight is a function of assimilation, respiration, growth of gonadal tissue, and resorption of gonadal tissue. Assimilation is a function of filtration and POC. Filtration is a function of a maximum filtration rate based on tissue weight, limited by sub-optimal temperature, salinity, TSS, O₂, and chl_a (Cerco and Noel, 2005; Fulford et al., 2007; Ehrich and Harris, 2015). The optimal temperature for oyster filtration (T_{opt}) is set to 27 °C (Jordan, 1987). Filtration is also multiplied by p , a tunable factor representing the proportion of computed filtration actually performed by oysters, which accounts for processes excluded from the model such as time spent filtering and is constrained by published growth rates. Respiration is a function of tissue weight, temperature, and assimilation. While filtration has a temperature limitation, respiration increases exponentially with temperature (Fig. S1). Tissue growth functions are not affected by

Deleted: in this

Deleted: the

Deleted: particulate organic carbon (

Deleted:)

carbonate chemistry variables, as experimental studies have found that neither filtration (Lemasson et al., 2018) nor respiration (Beniash et al., 2010; Matoo et al., 2013) of oysters are affected by pH changes; however, weight-specific net calcification is a function of Ω_{Ca} and temperature (Rivest et al., 2023). Shell growth is a function of both total tissue weight and net calcification.

2.2 Present day reference simulation

A realistic reference simulation was generated to represent 2017 conditions. The year 2017 was chosen for atmospheric, terrestrial, and open-ocean boundary conditions as this represents a relatively typical hydrological year. Atmospheric forcings (air temperature, long- and short-wave radiation, precipitation, winds, dewpoint temperature, and air pressure) are obtained from the ERA5 atmospheric reanalysis (Copernicus Climate Change Service, 2017; Hersbach et al., 2020). Surface atmospheric variables are available at 3-hourly intervals with a 0.25° resolution and are interpolated to a 0.2° grid. Terrestrial inputs of freshwater, nitrogen, carbon, and sediment are derived from the Phase 6 CBP Watershed Model (CBPWM; Bhatt et al., 2023) and USGS data. Daily estimates of freshwater discharge, water temperature, and loadings of nitrate, ammonium, organic nitrogen, and four classes of sediment from the CBPWM were concatenated to 74 locations throughout the model domain. To compute carbon loadings, constant carbon-to-nitrogen ratios are used, specifically 10:1 for dissolved organic matter (Hopkinson et al., 1998) and 6.625:1 for particulate organic matter (Redfield, 1934). Riverine TA concentrations are computed as in Da et al. (2024), using monthly-varying linear relationships between historical USGS observations of discharge and USGS TA estimates determined using the Weighted Regression on Time, Discharge, and Season (WRTDS; Hirsch et al., 2010) approach. Riverine DIC is calculated from daily riverine TA and daily DIC:TA ratios, linearly interpolated from the monthly climatology of USGS WRTDS DIC:TA in each tributary. Open boundary conditions are derived from a recent 600 m resolution whole-bay implementation of ROMS (St-Laurent and Friedrichs, 2024). Initial conditions for the six-month spin-up were derived from Da et al., (2024).

Deleted: (2023

Deleted: As in Da (2023), open

Deleted: previous model results (

Since spring-spawned oysters are typically deployed in late spring through summer on oyster farms, the reference run was started on July 1st and spanned one full year, ending June 30th of the following year. Oyster sizes were initialized based on shell height approximations of a typical spring-spawned oyster at deployment in July (i.e., a few months old). Starting dry tissue weight was assumed to be 0.001 g for all oysters, back-calculated from the approximate height of an oyster at the time of deployment. Starting shell dry weights and heights were calculated from allometric relationships to be 0.144 g and 11.6 mm, respectively.

2.3 Comparison of reference simulation to in situ observations

In situ water quality monitoring observations are available since 1984 throughout the Chesapeake Bay. Specifically, the Chesapeake Bay Program's Water Quality Monitoring Program (CBP WQMP) conducts cruises in the Bay and its tributaries. On average, stations are sampled once monthly, with the exception of June through August in the mainstem, when sampling occurs twice. In this study, measurements of water temperature, salinity, O₂, pH (NBS scale), TSS, and POC are

used from 16 CBP stations throughout the model domain, with depths ranging from 5 to 16 m (Fig. 1a; CBP, 2024). For all variables except TSS and POC, measurements are taken *in situ* using a YSI or Hydrolab® sonde roughly every one to two meters of the water column. TSS and POC are obtained from bottle samples at the surface, bottom, and at deeper stations, two additional depths above and below the pycnocline. TSS is determined by filtering a known volume of water through a pre-weighted filter and then re-weighing the filter after filtration and drying. POC is determined through combustion of a filter using an elemental analyzer (Olsen, 2012).

Model skill was evaluated by comparing results from the reference simulation to the CBP WQMP observations described above. Hourly outputs from the four closest grid cells to each CBP station were spatially interpolated to obtain results at each respective station. Multiple variables in ECB at the bottom level of the model, including temperature, salinity, O₂, pH, TSS, and POC, were compared with observations from the same station and time, within the bottom 10% of the water column (Table 1). Model bias and root-mean squared difference (RMSD) were computed for all aforementioned variables. Seasonal skill was also evaluated by comparing the 2017 reference run to CBP decadal averages. Decadal means were used for these comparisons, as once-monthly or once-seasonally sampling dates in 2017 bias outputs toward conditions on the time of the month when the measurements were taken in 2017, and the purpose of the comparison was to examine how the model reproduces average seasonal variability.

2.4 Future simulations

In addition to the reference run, this study generated five future simulations (Table 1) to investigate the change in carbonate chemistry conditions and oyster growth resulting from three drivers of future change in the bay: increased atmospheric CO₂ (*AtmCO₂*), atmospheric warming (*Temp*), and reduced nutrient loading (*TMDL*). Model forcings were modified for each simulation to represent mid-century conditions. A *Combined Future* simulation was run including forcings of all future stressors, in addition to three sensitivity simulations to isolate the impacts of each stressor on oyster growth. Atmospheric CO₂ concentration for the *AtmCO₂* and *Combined Future* simulations was set to 655 ppm, derived from the Coupled Model Intercomparison Project Phase 5 report RCP8.5 (business-as-usual) scenario projected for 50 years in the future relative to the reference run (Meinshausen et al., 2011). While it is reasonable to assume that warming temperatures will always accompany increases in atmospheric CO₂, separate experiments for each stressor were conducted. Isolating the physiological effects of each stressor helps us understand the mechanisms effecting the change in oyster growth and furthermore indicates the degree to which management strategies for offsetting acidification can reduce the effects of climate change on oysters. Future atmospheric temperature for the *Temp* and *Combined Future* simulations was obtained from the IPSL-CM5B-LR Earth System Model (Dufresne et al., 2013), statistically downscaled with the Multivariate Adaptive Constructed Analogs method (Abatzoglou and Brown, 2012). IPSL-CM5B-LR was selected as in Hinson et al. (2024), since it was deemed the most representative downscaled ESM of the 20 available (Hinson et al., 2023). As in Hinson et al. (2024), the delta method was used to calculate the daily average change in atmospheric temperatures between present-day and future conditions. To calculate this change, two 30-year climatologies, centered on 2000 and 2050 respectively, were computed and

Deleted: (Figs. 2, 3).

Formatted: English (UK)

Moved down [3]:), and similar to other model implementations of the Chesapeake Bay (Irby et al., 2016). Temperature and salinity are reproduced relatively well year-round (Fig.

Moved down [4]: Bottom O₂ and pH are slightly overestimated, exhibiting the greatest model-data misfit in the spring and summer months in the tributary channels (Fig.

Moved down [5]: .d). pH is overestimated by 0.2 units, which is within the accuracy of the electrode measurements. Observed POC concentrations in the York and upper Rappahannock are higher than simulated in the model and exhibit very high spatial variability (Fig.

Moved down [6]:). Despite the high spatial variability of the TSS observations (Fig.

Moved down [7]:), mean TSS ($45 \pm 54 \text{ mg L}^{-1}$) is captured within 1.1 mg L^{-1} by the model. Growth rates determined using the *EcoOyster* equations and environmental outputs from ROMS-ECB were compared with oyster data collected in the York River (Paynter et al., 2008; Liddel, 2008; Kingsley-Smith et al., 2009; Degremont et al., 2012; Callam et al., 2016). Specifically, the tunable parameter (p) that limits oyster filtration was adjusted to provide a best match between the modeled oyster growth rates and the published rates. Multiple p -values were tested, and a value of $p=0.15$ resulted in modeled oyster growth that best matched published growth rates. The resulting shell growth predicted by the model was found to be close to the *in situ* data ($52.0 \pm 1.1 \text{ mm y}^{-1}$ and $51.3 \pm 2.9 \text{ mm y}^{-1}$ for the model and observation means and standard deviations, respectively).

Deleted: When compared to 2017 WQMP observations and seasonal decadal averages, model skill of ROMS-ECBO is reasonably high (Table 1, Figs. 2, 3

Deleted: 2a,b) with annual biases of only 0.2°C and -1.5, respectively (Table 1).

Deleted: 2c

Deleted: 3a

Deleted: 3b

Deleted: 2

Formatted: Indent: First line: 0.5", Tab stops: Not at 3"

Deleted: CM5A

Deleted: 2023

Deleted: .

Deleted: 2023

357 daily averaged 50-year differences between the two climatologies (Fig. 2) were added to the atmospheric temperatures used
358 in the reference run. Future watershed inputs for the *TMDL* and *Combined Future* simulations included a climatology of nitrate,
359 ammonium, dissolved organic matter, and particulate organic matter concentrations, derived from a Phase 6 CBPWM 1991-
360 2000 run using reduced nutrient concentrations assuming the TMDLs had been successfully achieved (approximately a 20-
361 25% mean reduction in total nutrient loading; Bhatt et al., 2023). Freshwater discharge in this run was set to be identical to the
362 reference run, to isolate the effects of lowered nutrient concentrations on water chemistry and oyster growth. Since future
363 climate change is expected to impact terrestrial inputs much less than future management actions (Hinson et al., 2023), the
364 direct impact of climate change on the watershed is not considered in this analysis. A fifth simulation (*AtmCO₂ + Temp*) was
365 run to compare the influences of local management actions to the combined drivers of climate change, which includes both
366 future atmospheric CO₂ concentration and atmospheric temperature. Preliminary investigations revealed a minimal impact of
367 sea level rise on Ω_{Ca} in the bay; therefore, it was not included in the simulated climate change variables.
368 To generate open boundary conditions for each future simulation, a full bay model (St-Laurent and Friedrichs, 2024)
369 was run with the same atmospheric and river forcings as in this 120-meter model implementation. As in the reference run, all
370 future simulations were spun up for six months (January 1 – June 30) before beginning on July 1, but represent 50 years in the
371 future from the reference simulation (i.e., July 1, 2067). Initial conditions for all spin-ups are identical to the reference
372 simulation. Analysis confirmed the effects of initial conditions are negligible by July 1. To examine results most relevant to
373 oysters, model output was extracted at locations that support oyster production, defined as all grid cells in which tissue weight
374 exceeded 1 g at the end of the reference run (i.e., one year of growth; Fig. S2), which is inclusive of locations of active oyster
375 farms. All results shown are from the bottom level of the model, representing conditions similar to on-bottom or bottom cage
376 aquaculture methods that are common in Virginia. Spatial variation in model outputs across grid cells in the model domain is
377 reported using standard deviation.

378 **3 Results**

379 **3.1 Model Skill Assessment**

380 When compared to 2017 WQMP observations and seasonal decadal averages, model skill of ROMS-ECB is
381 reasonably high (Table 2, Figs. 3, 4), and similar to other model implementations of the Chesapeake Bay (Irby et al., 2016).
382 Temperature and salinity are reproduced relatively well year-round (Fig. 3a,b) with annual biases of only 0.2°C and -1.5,
383 respectively (Table 2). Bottom O₂ and pH are slightly overestimated, exhibiting the greatest model-data misfit in the spring
384 and summer months in the tributary channels (Fig. 3c,d). pH is overestimated by 0.2 units, which is within the accuracy of the
385 electrode measurements. Observed POC concentrations in the York and upper Rappahannock are higher than simulated in the
386 model and exhibit very high spatial variability (Fig. 4a). Despite the high spatial variability of the TSS observations (Fig. 4b),
387 mean TSS (45 ± 54 mg L⁻¹) is captured within 1.1 mg L⁻¹ by the model.

Deleted: 4

Deleted: ¶

Deleted: Irby

Deleted: 2018

Formatted: Font: 10 pt, English (US)

Deleted: S2).

Deleted: 3.1

Moved (insertion) [3]

Moved (insertion) [4]

Moved (insertion) [5]

Moved (insertion) [6]

Moved (insertion) [7]

Growth rates determined using the *EcoOyster* equations and environmental outputs from ROMS-ECB were compared with oyster data collected in the York River (Paynter et al., 2008; Liddel, 2008; Kingsley-Smith et al., 2009; Degremont et al., 2012; Callam et al., 2016). Specifically, the tunable parameter (p) that limits oyster filtration was adjusted to provide a best match between the modeled oyster growth rates and the published rates. Multiple p -values were tested, and a value of $p=0.15$ resulted in modeled oyster growth that best matched published growth rates. The resulting shell growth predicted by the model was found to be close to the *in situ* data (52.0 ± 1.1 mm y^{-1} and 51.3 ± 2.9 mm y^{-1} for the model and observation means and standard deviations, respectively).

3.2 Reference run results

In the present-day reference run, the environmental variables used as inputs to the oyster parameterizations exhibit substantial seasonal (Fig. 5a-f) and spatial (Figs. 6, S3) variability. As expected, bottom temperature is highest in summer, reaching an average of 29.3 °C in July when averaged across grid cells that support oyster growth (Fig. 5a). Temperature is higher in the shallower parts of the tributaries compared to the channels (Fig. S3a). Bottom salinity exhibits higher values in the fall and winter, reaching a maximum average of 17.7 in October, and drops in the spring and summer to reach a minimum average of 12.3 in June (Fig. 5b). Annual average bottom salinity ranges from 0 to 26 throughout the model domain (Fig. S3b), with the highest values in the southern areas in closest proximity to the open-ocean. The seasonal cycle for bottom POC is similar to that of temperature, peaking at 1.7 g C m^{-3} in June and dropping to 0.57 g C m^{-3} in January (Fig. 5c). Bottom POC also varies widely throughout the model domain (Fig. 6a), with relatively higher values in the Rappahannock compared to the York River, along the shoals of the tributaries, and along the western shoals of the mainstem Bay north of the Rappahannock. Ω_{Ca} exhibits an annual cycle similar to that of temperature and POC, reaching a maximum average of 3.2 in August and a minimum average of 1.1 in January (Fig. 5d). Annual mean bottom Ω_{Ca} also varies widely throughout the model domain (Fig. 6d). Generally, bottom Ω_{Ca} increases with salinity, with low to zero values in the tidal fresh portions of the upper tributaries and higher values along the western shoals of the mainstem Chesapeake Bay. The opposite temporal pattern is seen in bottom O_2 , which peaks at 12.3 mg L^{-1} in February and drops to an average of 6.3 mg L^{-1} in August (Fig. 5e). O_2 concentrations are highest along the shoals and lowest in the deep channels (Fig. S3c). Bottom TSS concentrations exhibit tidal variability throughout the year and are highest in the York River with much lower concentrations observed in the other portions of the model domain (Fig. S3d).

Tissue and shell weights increase modestly from July through April, and the highest rates of increase are seen in May and June near the end of the one-year reference run (Fig. 5g,h). At the end of the reference run, the spatial patterns of shell and tissue weight are nearly identical (Fig. 7), as tissue growth largely drives shell growth (Table S4). Both shell and tissue weights are highest along the shoals of the York and Rappahannock Rivers (Fig. 7a,d) and low in the deeper waters where TSS concentrations are high (Fig. S3d). A wider region of high shell and tissue weight appears in the Rappahannock, while the highest weights in the York are confined to a very narrow and shallow strip along the coastline. Shell and tissue weights are

Deleted: .

Deleted: Environmental conditions averaged annually across grid cells that support oyster growth are provided in Table 3, and conditions averaged annually across all grid cells in the model domain are provided in Table S5.

Formatted: English (UK)

431 higher along the southwestern than the northeastern coastlines of the tributaries, where the shoals are wider in both tributaries
432 (Fig. 1a).

433 **3.3 Results of Combined Future simulation**

434 All environmental variables examined exhibit change from the reference run in the *Combined Future* simulation.
435 Temperature and salinity are projected to increase across the entire model domain (Fig. S3a,b). When averaged over the model
436 domain, temperature is projected to increase by $1.5 \pm 0.26^{\circ}\text{C}$, and salinity is projected to increase by 0.21 ± 0.11 (Table S5).
437 Bottom POC is projected to decrease by $0.07 \pm 0.05 \text{ g C m}^{-3}$ (Table S5), with POC reductions predicted to be most pronounced
438 in the mid- to upper tributaries (Fig. 6c). Mid-century bottom Ω_{Ca} is projected to be lower throughout most of the region (Fig.
439 6f), with an average reduction of 0.8 ± 0.19 over the whole model domain (Table S5). The spatial distribution of future Ω_{Ca} is
440 generally consistent with present-day Ω_{Ca} patterns, and the greatest decreases are projected to occur in regions with the highest
441 present-day Ω_{Ca} (Fig. 6 d,e,f). An average reduction in O_2 of $0.3 \pm 0.08 \text{ mg L}^{-1}$ is predicted across the model domain (Table
442 S5), which will be mostly spatially uniform (Fig. S3c). TSS is projected to be reduced by $0.20 \pm 0.25 \text{ mg L}^{-1}$ with high spatial
443 variability in the projected change (Table S5; Fig. S3d).

444 Changes in environmental conditions do not occur uniformly throughout the year. Temporal changes in environmental
445 conditions averaged across grid cells that support oyster growth are provided in Figure 5. Annually averaged increases in
446 temperature and salinity are the same when averaged over only grid cells that support oyster growth as they are when averaged
447 across the entire model domain (Tables 3, S5). The greatest temperature increases are projected to occur in the warmer months,
448 with an average increase of 1.6°C predicted for June through August and an average increase of 1.2°C predicted for December
449 through February. Bottom temperatures are projected to surpass the optimal temperature for oyster filtration (27°C) primarily
450 in July and August (Fig. 5a). Salinity increases are projected to be greatest at the beginning of the year, with an average increase
451 of 0.44 between January and March and an average increase of 0.20 for the remainder of the year (Fig. 5b). Bottom POC at
452 grid cells that support oyster growth is expected to decrease slightly less than the average for the entire region (Tables 3, S5),
453 by an annual average of 0.09 g C m^{-3} , with the greatest reductions in the spring and summer and little to no change in the
454 winter (Fig. 5c). For Ω_{Ca} , O_2 , and TSS, projected reductions are slightly greater at oyster growth sites than for the entire domain.
455 Ω_{Ca} is projected to decrease by 0.9, with the greatest reductions expected to occur the warmer months (Fig. 5d). O_2 is projected
456 to decrease year-round, though with slightly greater reductions in the winter (Fig. 5e) and an annual average reduction of 0.4
457 $\text{mg O}_2 \text{ L}^{-1}$ (Table 3). TSS is projected to decrease annually by 0.3 mg L^{-1} (Table 3), mostly in the spring, due to lowered POC
458 (Fig. 5f).

459 Modeled shell and tissue weights after one year of growth are projected to decline in all regions that exhibit present-
460 day growth, with the most severe reductions (up to 100%) occurring along the York and Rappahannock River shoals (Figs.
461 7c,f, 8). One-year tissue weight will be reduced by 1.3 g, on average, representing a 60% reduction across grid cells that support
462 oyster growth (Table 4). Shell weight, which is largely driven by changes in tissue weight, is projected to be reduced by 11.4
463 g on average after one year of growth, representing a 68% reduction in average shell weight in regions that support oyster

Deleted: Oyster growth metrics averaged across grid cells that support oyster growth are provided in Table 4.
Formatted: Font: Bold, English (UK)
Deleted: 2

Deleted: ,

468 growth (Table 4). The greatest reduction in shell and tissue growth rates will occur in the warmer months near the end of the
469 one-year simulation (-0.1 g d⁻¹ from May through June), whereas the smallest change will occur in the winter months (-0.02 g
470 d⁻¹ from December through February), as the least growth occurs during that time (Fig. 5g,h). Shell thickness, calculated as
471 the ratio of shell weight to shell height, will be reduced by 61% on average (0.11 g mm⁻¹; Table 4).

472 Declines in year one shell weight will vary throughout the model domain (Fig. 8), following relative changes in
473 bottom POC and Ω_{Ca} (Fig. 9). The mainstem has the most moderate reduction in shell weight relative to reference shell weight,
474 with an average reduction of 31%, indicated by the slope of the scatterplot. Shell weights in the Rappahannock and York face
475 the steepest reductions relative to reference, with average reductions of 86% and 96%, respectively, and a large portion of
476 York oysters facing complete depletion of oyster tissue and shell in these locations (Fig. 9; indicated by proximity to 1:1 line).
477 Proportional shell weight reductions in the mainstem are projected to correlate with POC reductions (Fig. 9a). For Ω_{Ca} in the
478 mainstem, a group of sites face the greatest proportional reductions when Ω_{Ca} reductions are the greatest. However, for sites
479 with lower proportional shell loss, the opposite trend is observed (Fig 9d). In the Rappahannock, higher POC reductions
480 coincide with slightly lower proportional shell loss (Fig. 9b). Sites with the largest reductions in POC primarily occur in the
481 York (Fig. 9c; see dark blue symbols on the 1:1 line), and the greatest proportional shell weight reductions coincide with the
482 greatest POC and Ω_{Ca} reductions (Fig. 9c,f). Similar results are found for tissue weight (not shown).

483 **3.4 Results of individual future sensitivity simulations**

484 Four individual future sensitivity simulations were conducted to isolate the specific mechanisms (increased
485 atmospheric CO₂, increased atmospheric temperature, and/or nutrient reductions) causing the projected changes described
486 above in the *Combined Future* simulation. The *AtmCO₂* sensitivity simulation produces substantial reductions in average
487 bottom Ω_{Ca} (Fig. 10d) and, as expected, is not projected to substantially impact bottom temperature, salinity, POC, O₂, or TSS
488 (Table 3; Figs. 10a, S4). The projected reduction in Ω_{Ca} is 0.9 when averaged over oyster growth sites (Table 3), 0.1 greater in
489 magnitude than the average reduction for the entire model domain (Table S5), as greater reductions are expected along the
490 shoals of the Rappahannock and mainstem shoal than the York and upper section of the Rappahannock (Fig. 10d). In this
491 *AtmCO₂* simulation, shell weight is predicted to be most steeply reduced in the Rappahannock, with less impact in the York
492 and mainstem regions (Fig. 11a). At grid cells with oyster growth, *AtmCO₂* produces a shell weight reduction of 6.3 g and a
493 shell thickness reduction of 0.06 g mm⁻¹ in comparison to the reference simulation, but no change in tissue weight (Table 4).

494 The *Temp* sensitivity simulation produces changes in all environmental variables impacting oyster growth, with the
495 exception of Ω_{Ca} (Tables 3, S5). Average changes in temperature, salinity, and TSS will be identical to those from the
496 *Combined Future* simulation (Tables 3, S5). Predicted reductions in POC and O₂ will be smaller in magnitude than in
497 *Combined Future*, though more severe than any other single sensitivity experiment (Table 3, S5). Temperature and salinity
498 will increase across the entire model domain, with a greater salinity increase occurring in the Rappahannock and along the
499 mainstem shoal (Fig. S4a-c). TSS will decrease primarily in the channels of the lower York and Rappahannock and on the
500 mainstem shoal (Fig. S4d). POC reductions are expected to cover the majority of the model domain, with larger reductions in

Deleted: 3

Deleted:

Deleted: , 3

the upper Rappahannock (Fig. 10b). Slight increases in Ω_{Ca} are observed in shallow tidal creeks (Fig. 10e); however, no substantial change in average Ω_{Ca} is predicted (Table 3, S5). O_2 at oyster grid cells will exhibit a similar but slightly smaller average reduction compared to *Combined Future* (Table 3). Patterns of change in shell weight in the *Temp* sensitivity simulation resemble those in the *AtmCO₂* simulation (Figs. 7c, 11b), with additional reductions along the mainstem shoal and a greater predicted mean reduction of 7.1 g, a 42% decrease at grid cells with oyster growth (Table 4). Unlike *AtmCO₂*, tissue weight will decrease in *Temp*, by an average of 1 g, a 46% reduction (Table 4).

The *TMDL* sensitivity simulation produces a much smaller average change in environmental conditions than the *AtmCO₂* or *Temp* simulations (Tables 3, S5). *TMDL* does not substantially influence temperature, salinity, or O_2 (Tables 3, S4, S5), but produces POC and TSS reductions close to the averages for *Temp* (Tables 3, S5). While POC change in the *Temp* simulation is concentrated in the deeper portions of the tributaries (Fig. 10b), the POC reductions in the *TMDL* simulation are concentrated along the shoals of the tributaries, with the greatest reductions in the upper Rappahannock (Fig. 10c). TSS changes in *TMDL* are limited to the tributaries, occurring along the shoals of the Rappahannock and in patches throughout the York (Fig. S4d). Future change in Ω_{Ca} in this simulation is less than for *AtmCO₂* and is largely confined to the upper Rappahannock shoals and in shallow tidal creeks throughout the study region (Fig. 10d, f). Patterns of change in shell weight will resemble *AtmCO₂* and *Temp* in the tributaries, but no change is predicted along the mainstem shoal (Fig. 11a-c). The *TMDL* simulation produces reduced shell (3.7 g) and tissue (0.5 g) weights, with a smaller negative influence on shell and tissue weight than *Temp* (Table 4; Fig. 11b-f).

Environmental conditions in the *AtmCO₂* + *Temp* simulation are nearly identical to those in the *Temp* simulation (Tables 3, S5), with the exception of Ω_{Ca} , which is lower due to the influence of heightened atmospheric CO_2 . As tissue growth is unaffected by Ω_{Ca} , tissue weight in this simulation is identical to that of the *Temp* simulation (Table 4). Average shell weight reduction in *AtmCO₂* + *Temp* is 10.2 g, greater than that from *AtmCO₂* alone, due to the combined influences of lowered tissue growth and lower Ω_{Ca} (Table 4).

4 Discussion

This study provides high-resolution projections for oyster growing conditions and corresponding oyster growth in the Chesapeake Bay, with a specific focus on two Virginia tributaries. A high-resolution hydrodynamic-biogeochemical model was coupled with an Eastern oyster bioenergetics model and forced with future projections for atmospheric CO_2 , temperature, and nutrient management. An overall reduction in Ω_{Ca} and oyster growth are predicted by mid-century throughout the study region under the combined effects of all three future stressors. Specifically, the greatest reductions in oyster growth are projected to occur in the York and Rappahannock Rivers, where unfavorable conditions for calcification will expand in the future and where food availability will be strongly impacted by warming and nutrient reductions. Bottom conditions in the York and Rappahannock rivers, particularly in the upper portions, will likely be unsuitable for aquaculture at mid-century on average, indicating climate change preparedness is critical for the oyster aquaculture industry.

Deleted: Fig.

Deleted: , 3

Deleted: S5,

Deleted: Fig.

Deleted: , 3

Deleted: 10f

Deleted: 11c

Deleted: 11c, d

Deleted: Combined Future

Deleted: slightly higher

Deleted: absence of TMDL's

Deleted: .

Formatted: Font: Arial, 11.5 pt, Font color: Accent 1, Not Superscript/ Subscript

Formatted: Not Superscript/ Subscript

Deleted: .

Deleted: slightly

Deleted: .

551 **4.1 Future projections of Ω_{Ca}**

552 The magnitude of future change in Ω_{Ca} varies with present-day Ω_{Ca} conditions (Fig. 6d-f). Regions with high present-

553 day Ω_{Ca} , primarily the mainstem shoals, are projected to experience the greatest reductions because of their low partial pressure

554 of CO_2 (pCO_2) relative to fresher waters. Biologically driven low pCO_2 water on mainstem shoals has a greater capacity for

555 CO_2 uptake from the atmosphere than high pCO_2 water, which is causing the fresher tributaries to experience smaller increases

556 in DIC and smaller reductions in Ω_{Ca} (Fig. 6f). Acidic freshwater input often causes pCO_2 in the upper tributaries to exceed

557 atmospheric pCO_2 , causing outgassing (Cai et al., 2017; Shen et al., 2019b; St-Laurent et al., 2020; Cai et al., 2021). Despite

558 the lower Rappahannock having a lower salinity than the lower York, it also has a lower DIC to TA ratio, so the rate at which

559 the lower Rappahannock absorbs pCO_2 is higher (Da et al., 2021). Total alkalinity, or buffering capacity, is also lower in the

560 lower Rappahannock than the lower York (Da et al. 2021), so the lower Rappahannock cannot resist changes in carbonate

561 chemistry to the same degree as the York. As a result, we observe the Rappahannock changing faster than the York (Fig. 6f,

562 Fig. 9). Since higher Ω_{Ca} regions will experience greater reductions than lower Ω_{Ca} regions (Fig. 6d-f), the overall spatial

563 variability of Ω_{Ca} will be reduced by mid-century, and more areas will experience conditions that are unfavorable for oyster

564 shell-building (Fig. 5).

565 Although future atmospheric CO_2 and reduced nutrient loading will both contribute to Ω_{Ca} reductions, the modeling

566 experiments conducted here highlight that increasing atmospheric CO_2 is the largest contributor to decreases in Ω_{Ca} throughout

567 the study region. Increased atmospheric CO_2 will cause reductions in Ω_{Ca} across the model domain, while nutrient reductions

568 are expected to mainly influence Ω_{Ca} in shallow and fresh coastal areas, with little influence in oyster growing regions. The

569 effects of warming on Ω_{Ca} may slightly offset the influence of atmospheric CO_2 in certain areas, but this will likely only occur

570 in fresh tidal creeks where oysters do not currently reside (Fig. 10e). Given the importance of atmospheric CO_2 in shaping

571 future Ω_{Ca} conditions in the lower bay, reductions in anthropogenic carbon emissions will be necessary to lessen the projected

572 impacts on carbonate chemistry in the Chesapeake Bay and globally.

573 Comparing our results to other studies examining the effects of acidification reveals that the Chesapeake Bay will

574 likely acidify faster than the US West Coast. Siedlecki et al. (2021a) projected a decrease of 0.8-1.0 in Ω_{Ca} in the Northern

575 California Current System between 2000 and 2100, under the same future emissions scenario used in our study, i.e., RCP8.5.

576 Projections from the present work indicate a similar magnitude of reduction in the lower Chesapeake Bay over a shorter time

577 period (50 years), suggesting a faster rate of acidification in the lower bay. Feely et al. (2009) also reported that projections

578 for Ω_{Ca} reductions are slightly greater in the Atlantic than in the Pacific. The relative differences in rates of acidification should

579 be considered, however, in the context of present-day Ω_{Ca} . The Pacific Ocean has a higher ratio of DIC:TA than the Atlantic,

580 so present-day Pacific Ω_{Ca} is lower (Feely et al., 2004; Dunne et al., 2012). Therefore, while the Chesapeake Bay is acidifying

581 faster, coastal Pacific waters may become undersaturated with calcite and aragonite sooner than in Chesapeake Bay. US West

582 Coast shellfish mortality events associated with acidification or other climate change stressors may place increased pressure

583 on US Atlantic fisheries to provide shellfish to the nation, highlighting the importance of climate change preparedness and

584 resilience in the Chesapeake Bay region.

Formatted: Space Before: 0 pt, After: 0 pt, Line spacing: 1.5 lines

Deleted: .

Formatted: Font: Not Bold

Formatted: Font: Not Bold

Formatted: Heading 2, Line spacing: 1.5 lines

Deleted: .

Formatted: Font: Not Bold

Formatted: Font: Not Bold, English (US)

Deleted: .

Formatted: Font: Not Bold, English (US)

Deleted: .

Deleted: 5

Formatted: Font: Not Bold

Formatted: Font: Not Bold

Deleted: .

Deleted: .

592 While atmospheric CO₂ is primarily responsible for changes in Ω_{Ca} , nutrient reductions are also projected to worsen
593 carbonate chemistry conditions. Eutrophication can suppress acidification [in surface waters](#) by increasing primary production
594 (Borges and Gypens, 2010; Shen et al., 2019; Da et al., 2021), and when simulating a reduction in eutrophication via nutrient
595 management in our modeling study, the countering effect occurred. While the reduction in Ω_{Ca} from nutrient management is
596 minor compared to the projected impacts of CO₂-driven acidification, its small contribution may shift Ω_{Ca} conditions from
597 favoring net calcification to favoring net dissolution, demonstrating the importance of considering multiple drivers when
598 predicting exposure to ecologically relevant conditions of coastal acidification.

599 **4.2 Future projections of oyster growth**

600 Acidification, warming, and nutrient reductions are projected to affect shell and tissue growth of oysters in different
601 ways. Here, increased atmospheric CO₂ caused reductions in shell growth of Eastern oysters due to its negative effect on Ω_{Ca}
602 and thus calcification rates, which is consistent with experimental studies (Waldbusser et al., 2011; Gobler and Talmage, 2014;
603 Himes et al., 2024). Shell weight reductions from increased atmospheric CO₂ were driven by changes in calcification rate
604 alone, as tissue weight in *EcoOyster* is unaffected by Ω_{Ca} (Fig. 11d; Rivest et al., 2023). Experimental studies have identified
605 indirect physiological impacts of elevated CO₂ on juvenile/adult oyster metabolism, growth, and reproduction (Beniash et al.,
606 2010; Dickinson et al., 2012), suggesting that increased atmospheric CO₂ can sometimes influence tissue growth. Further
607 investigation is necessary in order to include the relationship between atmospheric CO₂ and oyster tissue growth in *EcoOyster*.
608 Biological and chemical reactions occur faster at higher temperatures, meaning calcification rates may be higher under future
609 warming conditions (Waldbusser et al., 2011), as long as Ω_{Ca} is still high enough to support calcification. Conversely, under
610 conditions of extreme low Ω_{Ca} , warming may exacerbate dissolution rates and shell weight reductions. Our results also show
611 that nutrient reductions will lead to reductions in shell weight, largely driven by a reduction in tissue weight resulting from
612 lower food availability (POC), rather than lower Ω_{Ca} .

613 While nutrient reductions are projected to have little influence on Ω_{Ca} in this study, their negative influence on food
614 availability may be detrimental to tissue growth in certain parts of the study region, particularly the York River. Our model
615 projections suggest that nutrient reductions may in some cases produce conditions that do not support any oyster growth along
616 the shoals of the York (Fig. 9c,d), a result of reductions in food availability that are predicted to be more substantial in the
617 tributaries than the mainstem region (Fig. 10c). Multiple studies have demonstrated that Eastern oysters and other calcifying
618 organisms perform better under acidification when they have sufficient food availability, as they are better able to keep up
619 with the energetic demands of environmental stress (Thomsen et al., 2015; Ramajo et al., 2016; Schwaner et al., 2023, [Caillon
620 et al., 2025](#)). Therefore, nutrient reductions will likely influence oyster growth under acidification stress by different
621 magnitudes in each tributary. When comparing the effects of local management actions to reduce nutrient runoff to the effects
622 of climate change (increased atmospheric CO₂ and warming), it is evident that, on average, climate change will have a much
623 greater negative influence on oyster growth (Table 4). However, the strong localized impacts of nutrient reductions in the York

Deleted: ; 10c

Deleted: 6c

Deleted:).

627 highlight the importance of examining the spatial variability of future changes in oyster growth. It is important for managers
628 to consider local conditions when assessing the effects of nutrient reductions on oyster production.

629 Increased water temperatures are projected to slow oyster growth in the future. Specifically, large reductions in tissue
630 weight are underpinned by three primary mechanisms: limitations on filtration at high temperatures (Loosanoff, 1958),
631 increased respiration rates (Dame, 1972), and reduced food availability. In *EcoOyster*, the optimal temperature for Eastern
632 oyster filtration is 27°C (Cерco et al., 2005; Jordan, 1987), and under warming, the frequency at which ambient summer
633 temperatures will surpass this optimal temperature will be higher (Fig. 5a), therefore causing more frequent declines in
634 filtration rate (Cерco et al., 2005; Fulford et al., 2007). There is no clear optimal temperature for oyster respiration, and
635 therefore it is assumed to increase exponentially with temperature (Hochachka and Somero, 2002). Thus, as oyster filtration
636 rates begin to decline at high temperatures, respiration rates will continue to rise and decrease the potential for tissue
637 accumulation (Fig. S1). Previous studies on juvenile Eastern oysters do not support a consensus on the relationship between
638 warming and tissue growth. Some report that growth is inhibited at higher temperatures (31°C, Stevens and Gobler, 2018;
639 30°C, Speights et al., 2017). In contrast, Talmage and Gobler (2011) found no significant influence of high temperature (28°C)
640 alone on tissue growth. The optimal temperature for oyster filtration may also vary among oysters, based on observations of
641 maximum filtration rates of adult Eastern oysters occurring between 28.1°C– 32°C (Loosanoff, 1958). Variation in
642 experimental design may have contributed to the contrast in results summarized here, in addition to the influence of local
643 adaptation (Burford et al., 2014). Other studies that incorporate higher temperature thresholds into their models predict
644 increases in oyster biomass under warming in Chesapeake Bay (Allen et al., 2023), underscoring the importance of properly
645 parameterizing growth models. Additional modeling studies should be conducted to test the sensitivity of oyster growth
646 changes to optimal temperature parameterizations. Due to a lack of consensus on temperature limits of Eastern oyster filtration,
647 further research is also needed to more robustly represent oyster filtration in bioenergetics models and improve predictions of
648 impacts of warming on oysters and their ecosystem services in the region.

649 Warming will likely have a negative effect on food availability for oysters. Compared to the effects of nutrient
650 reductions, warming will have a much more widespread influence on POC, causing reductions throughout the model domain
651 (Fig. 10b,c). Despite warming increasing rates of POC production via increased phytoplankton growth rates, factors such as
652 nutrient limitation and increased respiration rates will result in a net decrease in POC availability. In the tributaries, reductions
653 in food availability will be most widespread due to warming, but less extreme than those from nutrient reductions in the shallow
654 parts of the tributaries where oysters are affected. Remineralization of organic carbon in marine systems is temperature-
655 dependent (López-Urrutia et al., 2006), and as warming occurs, remineralization of detrital carbon to DIC in bottom waters
656 will occur at higher rates. As much of the lower bay is nutrient-limited (Zhang et al., 2021), phytoplankton growth rates will
657 not increase much from warming alone; therefore, increased remineralization will likely reduce the overall amount of food
658 available to oysters. Despite a similar average reduction in food availability being predicted for the future warming simulation
659 and managed nutrient reductions simulation, the influence of warmer temperatures will amplify the negative effects of reduced
660 food availability on growth. In this study, the critical temperature at which respiration rates exceed assimilation rates is

Deleted: 7a

662 dependent on filtration. When food availability limits filtration, this critical temperature lowers, and the temperature threshold
663 for tissue loss is lowered. Experimental studies have demonstrated how organic carbon may be influenced by both warming
664 and acidification (Simone et al., 2021), but as these dynamics can differ based on nutrient availability, it is important to consider
665 how climate change will influence food webs and nutrient dynamics.

666 The projected mid-century reductions in oyster growth obtained from this analysis are consistent with the results of
667 other studies that examine oyster growth under similar projected climate change conditions. A study modeling oyster responses
668 to warming and low salinity co-stressors in Barataria Bay, LA, for example, predicts that under a warming and high flow
669 scenario (though without the effects of future nutrient reductions or atmospheric CO₂), oysters will experience widespread
670 mortality in fresher parts of the bay by the end of the century (Lavaud et al., 2021). Experimental studies have shown similar
671 negative effects of acidification, warming, lower food availability, and increased freshwater flow on oyster survival (La Peyre
672 et al., 2013; Rybovich et al., 2016; Lowe et al., 2019; Jones et al., 2019). Da (2023) found that the reductions in salinity and
673 Ω_{Ca} that result from high discharge events in the York River will increase in extent as climate change progresses and
674 increasingly threaten aquaculture production. In the Chesapeake Bay, extreme precipitation events are predicted to occur more
675 frequently with future climate change, however an overall decline in annual average precipitation is also predicted (St. Laurent
676 et al., 2021). As a result, the overall impact of freshwater from the land is not projected to change significantly in the future
677 (Hinson et al., 2023). Changes in precipitation were thus not simulated in this study, but future work could examine the
678 dynamics of climate change, salinity, Ω_{Ca} , and oyster growth in a year with more heavy rainfall events but lower annual rainfall.

679 4.3 Influence of future changes in oyster growth on aquaculture

680 Understanding the relative impacts of global climate change and local nutrient management actions on oyster growth
681 and survival will allow aquaculture producers to anticipate how their oyster stock may respond to these anthropogenic changes.
682 As the effects of climate change are subject to natural interannual variability, the magnitude of acidification and warming in a
683 given year will likely differ (Cai et al., 2021; Moore-Maley et al., 2016; Li et al., 2016), influencing oyster growth through
684 differing mechanisms. Smaller oysters resulting from slower growing times in a particularly warm year may present a different
685 challenge to growers than weak-shelled oysters in a year with lower Ω_{Ca} and average temperatures. Mortality may also become
686 a more urgent challenge as summer temperatures warm. A previous study examining commercial performance of Pacific
687 oysters in Brazil found that interannual variability in temperature, chl *a* abundance, and climate events influenced survival and
688 growth phase timing (Mizuta et al., 2012). High temperatures inhibited survival of oyster seed in that study, which frequently
689 occurs in Pacific oysters (*Crassostrea gigas*) during the summer months in Europe and California (Goulletquer et al., 1998;
690 Burge et al., 2007; Malhan et al., 2009). A similar phenomenon has been observed in Eastern oysters; however, mortality
691 events in this species have not been conclusively linked to warmer water temperatures (Guevelou et al., 2019; Biranik and
692 Allam, 2023), and the cause is yet to be resolved for either species, and remains an area of active research. Nonetheless, the
693 increasing occurrence of spring/summer mortality in Eastern oysters suggests that shifting the time of planting oysters on

Deleted: .

695 leases later in the year may help mitigate the risk of widespread mortality, although the economic tradeoffs involved in shifting
696 the growing season for oysters should be taken into account.

697 Future climate change and nutrient management are projected to worsen conditions for oyster growth, and the spatial
698 variation in these changes may unevenly influence aquaculture production. While reductions in shell and tissue growth are
699 predicted for nearly all regions where oysters grow, these changes will likely differ based on present-day environmental
700 conditions. Under present day conditions, the most oyster growth is projected to occur in regions with some of the highest
701 present-day Ω_{Ca} and the greatest projected Ω_{Ca} reductions, i.e., in the Rappahannock River and mainstem shoals. Some of the
702 most dramatic tissue and shell reductions are projected to occur in the York and upper Rappahannock, where reduced food
703 availability and low Ω_{Ca} will limit oyster filtration and shell growth. Oysters in parts of both the Rappahannock and York
704 Rivers will likely face mortality (represented by near complete depletion of oyster shell and tissue) by mid-century (Figs. 8,
705 9). However, these reductions will not be spatially uniform, underscoring the importance of oyster farm site selection within a
706 tributary. In contrast, oysters grown outside the tributaries are projected to exhibit a smaller decline in growth, indicating
707 greater future opportunity for oyster farming in these locations. Under the business-as-usual climate change trajectory analyzed
708 here, bottom conditions in the tributaries will be less suitable for oyster aquaculture by mid-century, and producers might
709 consider alternate farm locations or shifting production methods toward floating culture to avoid exposure to low Ω_{Ca}
710 conditions and access greater food availability.

711 Beyond reduced oyster growth, aquaculture operations may also be affected in the future by temporal changes in
712 optimal growing conditions. Due to the input of freshwater that lowers DIC and TA and increases pCO_2 (Cai et al., 2017; Cai
713 et al., 2021; Da et al., 2024), the greatest magnitude of Ω_{Ca} reductions occurs in spring. The majority of oyster growth is
714 projected to occur in the spring and summer (Fig. 5), so changes to growing conditions may be most consequential during
715 these warmer months. Deployment of oyster seed generally begins in the spring and continues into the summer, so it is
716 important for producers to be aware of ambient conditions being experienced by their newly deployed oysters. As spring
717 temperatures warm, phytoplankton blooms will likely occur earlier in the year, shifting the time when food availability is
718 highest (Da et al., 2021). Oysters deployed earlier in the year may benefit from greater food availability and perform better
719 than oysters deployed in July or August when waters are warmest. However, they may also face the challenge of spring/summer
720 mortality events, revealing the complexity of timing oyster deployment under worsening climate change conditions. For oyster
721 farms closer to freshwater sources, the combined effects of low Ω_{Ca} , low salinity, and high summer temperatures may severely
722 inhibit growth and extend time-to-market. This study focused on diploid oysters, since the laboratory experiments used to
723 develop the EcoOyster model parameterizations were conducted on diploids. Future laboratory experiments with triploids
724 would enhance our modeling efforts for triploid oysters, which are commonly used in aquaculture in the Chesapeake Bay
725 region.

Deleted: 7

727 4.4 Future work

728 Providing the aquaculture industry with the best existing estimates of climate change impacts to their operations will
729 allow them to make more informed decisions about their future practices. This study used a 120-meter horizontal resolution
730 model grid to examine near-lease-level effects of climate change and management actions on oyster growth in a section of the
731 lower Chesapeake Bay. Similar studies with high resolution model grids in other systems will strengthen our understanding of
732 how regional anthropogenic effects will influence the oyster aquaculture sector and could be used to identify areas of
733 opportunity for new aquaculture practices (Swam et al., 2022; Palmer et al., 2021; Lavaud et al., 2024). The present study
734 incorporated one Earth System Model and one emissions scenario; future work should quantify how these choices impact
735 estimates of future Ω_{Ca} and oyster growth (e.g., Hinson et al., 2023). Future modeling studies should also incorporate other
736 climate change impacts, such as sea level rise and increased storminess which are projected to influence conditions for oyster
737 growth in the Chesapeake Bay region (Seneviratne et al., 2012; Lowe et al., 2019; Rybovich et al., 2016; Jones et al., 2019).

738 To improve estimates of shell and tissue growth of oysters under climate change, additional experimental studies
739 should be conducted to reduce the data gaps that currently limit model formulations. Uncertainties in the functional
740 relationships and rate parameters used in these models may lead to an inaccurate influence of some environmental variables
741 on oyster growth. For example, results in this study may be particularly sensitive to the optimum temperature for filtration
742 rate. Reductions in tissue weight are particularly dramatic when average temperature conditions at oyster lease sites remain
743 above this optimal temperature from mid-June through late August, a vital time for oyster growth. Many physiological studies
744 of temperature impacts on oyster filtration date back to the mid-to-late-20th century, and present-day seasonal extremes that
745 coastal organisms experience may routinely exceed the maximum temperatures used in many of these earlier experimental
746 designs. For example, Jordan (1987) used a maximum temperature of 27 °C, which was the ambient temperature when samples
747 were collected in July from the Choptank River, MD. Between 1985 and 2014, bottom waters of the north mesohaline Bay
748 main stem (closest to the Choptank) warmed 1.01 ± 0.13 °C during May to October (Hinson et al., 2022), and the present study
749 predicts a 1.5 ± 0.26 °C increase across the entire model domain between 2017 and mid-century. To build stronger models of
750 future climate impacts, and to expand scientific understanding of physiological limits of the Eastern oyster, future studies
751 should re-examine temperature limitations on oyster filtration and respiration by using higher experimental temperatures.

752 As oyster growth is highly sensitive to food availability, improved measurements of particulate organic carbon in the
753 region would fortify projections of oyster production under future climate change and nutrient management. Here, it is assumed
754 that oysters feed on POC, a combination of plankton and detritus. However, average POC concentrations are highly
755 spatiotemporally variable in the Chesapeake Bay due to eutrophication and algal blooms. In this study, POC was
756 underestimated in the tributary channels; however, it is unclear how well POC was estimated in oyster growing areas, as *in*
757 *situ* measurements are currently limited to stations in the channels during monthly or semi-monthly sampling cruises. More
758 routine POC measurements, as well as measurements of POC in regions where oyster farming operations occur, are needed to

Deleted: As a result, growth in the model is sensitive to the simulation start date, and future studies should compare the influence of warming on growth in simulations that start at different times in the year.

763 verify the spatiotemporal dynamics of food availability. Improved measurements of oyster food availability would allow for
764 stronger model skill assessment and improved projections of oyster production.

765 **5 Conclusions**

766 This study predicts widespread reductions in Ω_{Ca} in the lower Virginia tributaries of the Chesapeake Bay by mid-
767 century, highlighting the use of high-resolution model projections to better understand present-day carbonate chemistry
768 conditions and to predict the effects of climate change on a region of high interest for aquaculture production. While similar
769 modeling studies have projected acidification conditions in coastal regions with 3D coupled models (Siedlecki et al., 2021a,b;
770 Fujii et al., 2023) or modeled oyster growth with remote-sensing data and dynamic energy budget models (Palmer et al., 2020;
771 Palmer et al., 2021; Bertollini et al., 2021), the present study projects both carbonate chemistry conditions and oyster
772 bioenergetics in the Chesapeake Bay with the highest resolution thus far. Specifically, widespread reductions in Ω_{Ca} will
773 negatively impact oyster growth, with implications for aquaculture operations and local and regional economies. As bottom
774 conditions worsen, altered site-selection for oyster farms or other adaptive measures will become imperative to sustain
775 production and reduce the impacts of low Ω_{Ca} on farmed oysters.

776 Increased atmospheric CO₂ and nutrient reductions are projected to inhibit oyster calcification, while warming and
777 nutrient reductions will reduce oyster tissue and shell growth due to limitations on filtration and lowered food availability.
778 While the effects of global climate change on oyster growth are projected to be much stronger overall than the effects of local
779 nutrient management, lowered food availability from nutrient reductions may have a strong influence on oyster growth in
780 certain parts of the study region. As a result, all areas will not be equally vulnerable to future changes in the atmosphere and
781 watershed. Understanding how individual drivers influence oyster growth is important for predicting effects on aquaculture
782 production in the context of interannual variability of climate change and nutrient management outcomes. While the negative
783 effects of temperature on growth were strong in this study, additional studies on Eastern oyster temperature limits are needed
784 to improve projections, particularly as summer mortality of oysters is already common. Increased *in situ* measurements of
785 biogeochemical variables and experimental studies on oyster physiology and bioenergetics will allow for improved projections
786 of mid-century conditions and their potential impacts on oyster growth and the aquaculture industry.

787 **Code Availability**

788 Model code will be available upon request.

791 **Data Availability**

792 Model output will be available with a DOI on William & Mary ScholarWorks.

794 **Author Contribution**

795 MAMF, EBR, MJB, and PS wrote the proposal and acquired the funding for the project; MAMF, PS, and FD developed the
796 ROMS-ECB code; MJB developed the EcoOyster code; CC, MAMF, and EBR designed the experiment; CC ran model
797 simulations, analyzed the output, created the figures, and wrote the manuscript draft; MAMF, EBR, MJB, PS, and FD reviewed
798 and edited the manuscript.

799

800 **Competing Interests**

801 The authors declare that they have no conflict of interest.

802

803 **Acknowledgements**

804 This paper is the result of research funded by the National Oceanic and Atmospheric Administration's Ocean Acidification
805 Program under award NA18OAR0170430 to the Virginia Institute of Marine Science (VIMS). We would like to thank the
806 VIMS and William & Mary (W&M) high performance computing group for their technical support and computing resources.
807 We also thank the NOAA Chesapeake Bay Program for providing us with watershed inputs from their Phase 6 Watershed
808 Model. This work was largely made possible by Sara Blachman's hard work on the EcoOyster model. We thank Bill Walton
809 for his aquaculture expertise and support throughout the project. The model results used for this manuscript are available at
810 W&M Scholarworks.

811 **References**

812 Abatzoglou, J. T. and Brown, T. J.: A comparison of statistical downscaling methods suited for wildfire applications, *Int. J.*
813 *Clim.*, 32, 772–780, <https://doi.org/10.1002/joc.2312>, 2012.

814 Allen, K. L., Ihde, T., Knoche, S., Townsend, H., & Lewis, K. A.: Simulated climate change impacts on striped bass, blue crab
815 and Eastern oyster in oyster sanctuary habitats of Chesapeake Bay. *Estuar. Coast. Shelf Sci.*, 292, 108465,
816 <https://doi.org/10.1016/j.ecss.2023.108465>, 2023.

817 Amaral, V., Cabral, H. N., and Bishop, M. J.: Effects of estuarine acidification on predator–prey interactions. *Mar. Eco. Prog.*
818 *Ser.*, 445, 117–127, <https://doi.org/10.3354/meps09487>, 2012.

819 Barclay, K.M., Gingras, M.K., Packer, S.T. and Leighton, L.R.: The role of gastropod shell composition and microstructure in
820 resisting dissolution caused by ocean acidification, *Mar. Environ. Res.*, 162, 105105,
821 <https://doi.org/10.1016/j.marenvres.2020.105105>, 2020.

822 Barton, S. and Yvon-Durocher, G.: Quantifying the temperature dependence of growth rate in marine phytoplankton within
823 and across species, *Limnol. Oceanogr.*, 64, 2081–2091, <https://doi.org/10.1002/lno.11170>, 2019.

824 Beniash, E., Ivanina, A., Lieb, N., Kurochkin, I., and Sokolova, I.: Elevated level of carbon dioxide affects metabolism and
825 shell formation in oysters *Crassostrea virginica* (Gmelin), *Mar. Ecol. Prog. Ser.*, 419, 95–108,
826 <https://doi.org/10.3354/meps08841>, 2010.

Moved down [8]: Table 1.

Moved down [9]: Model skill statistics (mean ± standard deviation) comparing bottom grid cells from the reference run to Chesapeake Bay Program observations from the same station location and time, within the bottom 10% of the water column.

Moved down [10]: Table 2.

Moved down [11]: Table 3. Bottom environmental variables for each model simulation (annual mean ± standard deviation) for grid cells that support oyster growth in the reference run (defined as those with greater than 1g dry tissue weight after one year of growth; Fig. S2). Analogous results averaged over all model grid cells are shown in Table S5.

Moved down [12]: Figure 1. ROMS-ECBO model domain of Chesapeake Bay tributaries illustrating (a) bathymetry in meters and locations of Chesapeake Bay Program (CBP) water quality monitoring stations (red circles) and (b) bottom salinity zones.

Moved down [13]: Seasonally-averaged bottom (a) POC and (b) TSS from output of the reference run of the ROMS-ECBO model. Circles represent seasonal decadal-averaged bottom measurements at Chesapeake Bay Program stations (2010–2020). (DJF = winter, MAM = spring, JJA = summer, and SON = fall).

Moved down [14]: Figure 6. Annual mean bottom (a–c) POC and (d–f) Ω_{Ca} from (a,d) the present-day reference run, (b,e) the *Combined Future* simulation, and (c,f) the difference between (a) and (b), i.e., *Combined Future* minus reference.

Moved down [15]: Figure 10. Differences in annual averaged (a–c) bottom POC and (d–f) bottom Ω_{Ca} (d–f) for three sensitivity experiments: (a) $AtmCO_2$, (b) Temp, and (c) TMDL. Differences represent future results minus those from the present-day reference run.

Deleted: Captions

Deleted: Experimental design for future simulations conducted for comparison to reference run. Model forcings include a combination of 2017 (reference) and 2067 (future) inputs of atmospheric CO_2 , atmospheric temperature, and terrestrial nutrient loadings.

Deleted: Table 4. Modeled oyster characteristics from the end of each simulation (mean ± standard deviation) over grid cells that support oyster growth in the reference run (defined as those with greater than 1g dry tissue weight after one year of growth; Fig. S2).

Deleted: Figure 2. Seasonally-averaged bottom (a) temperature, (b) salinity, (c) dissolved oxygen, and (d) pH from the reference run. ... [3]

Deleted: Figure 7. (a–c) Shell weight and (d–f) tissue weight at the end of the one-year simulation from (a,d) the present-day reference run. ... [5]

Deleted: ... [6]

Formatted: Font: +Body (Times New Roman), Bold

Formatted: Font: +Body (Times New Roman)

Formatted: Font: Bold

Formatted: Font: Bold

914 Bertolini, C., Brigolin, D., Porporato, E. M. D., Hattab, J., Pastres, R., and Tiscar, P. G.: Testing a Model of Pacific Oysters'
 915 (*Crassostrea gigas*) Growth in the Adriatic Sea: Implications for Aquaculture Spatial Planning, *Sustainability*, 13, 3309,
 916 <https://doi.org/10.3390/su13063309>, 2021.

917 Bhatt, G., Linker, L., Shenk, G., Bertani, I., Tian, R., Rigelman, J., Hinson, K., and Claggett, P.: Water quality impacts of
 918 climate change, land use, and population growth in the Chesapeake Bay watershed, *JAWRA J. Am. Water Resour. Assoc.*, 59,
 919 1313–1341, <https://doi.org/10.1111/1752-1688.13144>, 2023.

920 Borges, A. V. and Gypens, N.: Carbonate chemistry in the coastal zone responds more strongly to eutrophication than to ocean
 921 acidification, *Limnol. Oceanogr.*, 55, 346–353, <https://doi.org/10.4319/lo.2010.55.1.0346>, 2010.

922 Boulais, M., Chenevert, K. J., Demey, A. T., Darrow, E. S., Robison, M. R., Roberts, J. P., and Volety, A.: Oyster reproduction
 923 is compromised by acidification experienced seasonally in coastal regions, *Sci. Rep.*, 7, 13276, [https://doi.org/10.1038/s41598-](https://doi.org/10.1038/s41598-017-13480-3)
 924 017-13480-3, 2017.

925 Brianik, C. J. and Allam, B.: The need for more information on the resistance to biological and environmental stressors in
 926 triploid oysters, *Aquaculture*, 577, 739913, <https://doi.org/10.1016/j.aquaculture.2023.739913>, 2023.

927 Bukaveckas, P. A.: Carbon dynamics at the river–estuarine transition: a comparison among tributaries of Chesapeake Bay,
 928 *Biogeosciences*, 19, 4209–4226, <https://doi.org/10.5194/bg-19-4209-2022>, 2022.

929 Brush, M.J., and M.L. Kellogg: Harris Creek Oyster Restoration Model v2. Virginia Institute of Marine Science, Gloucester
 930 Point, VA, <https://www.vims.edu/research/departments/bio/programs/sempr/models/index.php>, 2018.

931 Burford, M., Scarpa, J., Cook, B., and Hare, M.: Local adaptation of a marine invertebrate with a high dispersal potential:
 932 evidence from a reciprocal transplant experiment of the eastern oyster *Crassostrea virginica*, *Mar. Ecol. Prog. Ser.*, 505, 161–
 933 175, <https://doi.org/10.3354/meps10796>, 2014.

934 Burge, C. A., Judah, L. R., Conquest, L. L., Griffin, F. J., Cheney, D. P., Suhrbier, A., Vadopalas, B., Olin, P. G., Renault, T.,
 935 and Friedman, C. S.: Summer seed mortality of the pacific oyster, *Crassostrea gigas* (Thunberg) grown in Tomales Bay,
 936 California, USA: the influence of oyster stock, planting time, pathogens, and environmental stressors, *J. Shellfish Res.*,
 937 <https://doi.org/10.2983/0730-8000>, 2007.

938 Cai, W., Feely, R. A., Testa, J. M., Li, M., Evans, W., Alin, S. R., Xu, Y.-Y., Pelletier, G., Ahmed, A., Greeley, D. J., Newton,
 939 J. A., and Bednaršek, N.: Natural and Anthropogenic Drivers of Acidification in Large Estuaries, *Annu. Rev. Mar. Sci.*,
 940 <https://doi.org/10.1146/annurev-marine-010419-011004>, 2021.

941 Cai, W.J., Huang, W.-J., Luther, G. W., Pierrot, D., Li, M., Testa, J., Xue, M., Joesoef, A., Mann, R., Brodeur, J., Xu, Y.-Y.,
 942 Chen, B., Hussain, N., Waldbusser, G. G., Cornwell, J., and Kemp, W. M.: Redox reactions and weak buffering capacity lead
 943 to acidification in the Chesapeake Bay, *Nat. Commun.*, 8, 369, <https://doi.org/10.1038/s41467-017-00417-7>, 2017.

944 Cai, W.J., Xu, Y.-Y., Feely, R. A., Wanninkhof, R., Jönsson, B., Alin, S. R., Barbero, L., Cross, J. N., Azetsu-Scott, K.,
 945 Fassbender, A. J., Carter, B. R., Jiang, L.-Q., Pepin, P., Chen, B., Hussain, N., Reimer, J. J., Xue, L., Salisbury, J. E.,
 946 Hernández-Ayón, J. M., Langdon, C., Li, Q., Sutton, A. J., Chen, C.-T. A., and Gledhill, D. K.: Controls on surface water

carbonate chemistry along North American ocean margins, *Nat. Commun.*, 11, 2691, <https://doi.org/10.1038/s41467-020-16530-z>, 2020.

Cai, W. J., and Wang, Y.: The chemistry, fluxes, and sources of carbon dioxide in the estuarine waters of the Satilla and Altamaha Rivers, Georgia. *Limnol. Oceanogr.*, 43(4), 657–668, <https://doi.org/10.4319/lo.1998.43.4.0657>, 1998.

Caldeira, K. and Wickett, M. E.: Anthropogenic carbon and ocean pH, *Nature*, 425, 365–365, <https://doi.org/10.1038/425365a>, 2003.

Caillon, C., Fleury, E., Di Poi, C., Gazeau, F., and Pernet, F.: Food availability, but not tidal emersion, influences the combined effects of ocean acidification and warming on oyster physiological performance, *Aquaculture*, 742459, <https://doi.org/10.1016/j.aquaculture.2025.742459>, 2025.

Caldeira, K. and Wickett, M. E.: Ocean model predictions of chemistry changes from carbon dioxide emissions to the atmosphere and ocean, *J. Geophys. Res.: Oceans*, 110, <https://doi.org/10.1029/2004jc002671>, 2005.

Callam, B. R., Allen, S. K., and Frank-Lawale, A.: Genetic and environmental influence on triploid *Crassostrea virginica* grown in Chesapeake Bay: Growth, *Aquaculture*, 452, 97–106, <https://doi.org/10.1016/j.aquaculture.2015.10.027>, 2016.

Carstensen, J. and Duarte, C. M.: Drivers of pH Variability in Coastal Ecosystems, *Environ. Sci. Technol.*, 53, 4020–4029, <https://doi.org/10.1021/acs.est.8b03655>, 2019.

Cerco, C. and Noel, M.: Process-based primary production modeling in Chesapeake Bay, *Mar. Ecol. Prog. Ser.*, 282, 45–58, <https://doi.org/10.3354/meps282045>, 2004.

Cerco, C. F. and Noel, M. R.: Nonnative Oysters in the Chesapeake Bay, 2005.

Cerco, C. F., Noel, M. R., and Wang, P.: The Shallow-Water Component of the Chesapeake Bay Environmental Model Package, *JAWRA J. Am. Water Resour. Assoc.*, 49, 1091–1102, <https://doi.org/10.1111/jawr.12106>, 2013.

Chesapeake Bay Program DataHub: <https://datahub.chesapeakebay.net/>, last access: 28 January 2024

Comeau, L. A., Mayrand, É., and Mallet, A.: Winter quiescence and spring awakening of the Eastern oyster *Crassostrea virginica* at its northernmost distribution limit, *Mar. Biol.*, 159, 2269–2279, <https://doi.org/10.1007/s00227-012-2012-8>, 2012.

Copernicus Climate Change Service: ERA5: Fifth Generation of ECMWF Atmospheric Reanalyses of the Global Climate, Copernicus Climate Change Service Climate Data Store (CDS). <https://cds.climate.copernicus.eu/cdsapp#!/home>, 2017.

Da, F., Friedrichs, M. A. M., St-Laurent, P., Shadwick, E. H., Najjar, R. G., and Hinson, K. E.: Mechanisms Driving Decadal Changes in the Carbonate System of a Coastal Plain Estuary, *J. Geophys. Res.: Oceans*, 126, <https://doi.org/10.1029/2021jc017239>, 2021.

Da, F.: Chesapeake Bay Carbon Cycle: Past, Present, Future, PhD. Dissertation, Virginia Institute of Marine Science, William & Mary, Virginia, USA, <https://dx.doi.org/10.25773/v5-46f7-e286>, 2023.

Da, F., Friedrichs, M. A. M., St-Laurent, P., Najjar, R. G., Shadwick, E. H., and Stets, E. G.: Influence of Rivers, Tides, and Tidal Wetlands on Estuarine Carbonate System Dynamics, *Estuaries Coasts*, 1–23, <https://doi.org/10.1007/s12237-024-01421-z>, 2024.

980 Dame, R.F.: The ecological energies of growth, respiration and assimilation in the intertidal American oyster *Crassostrea*
981 *virginica*, *Mar. Biol.*, 17, 43-250, 1972.

982 Dayton, P.K.: Toward an understanding of community resilience and the potential effects of enrichments to the benthos at
983 McMurdo Sound, Antarctica, *Proceedings of the colloquium on conservation problems in Antarctica*, 81-96, 1972.

984 Dégremont, L., Garcia, C., Frank-Lawale, A., and Allen, S. K.: Triploid Oysters in the Chesapeake Bay: Comparison of Diploid
985 and Triploid *Crassostrea virginica*, *J. Shellfish Res.*, 31, 21–31, <https://doi.org/10.2983/035.031.0103>, 2012.

986 Dickinson, G. H., Ivanina, A. V., Matoo, O. B., Pörtner, H. O., Lannig, G., Bock, C., Beniash, E., and Sokolova, I. M.:
987 Interactive effects of salinity and elevated CO₂ levels on juvenile eastern oysters, *Crassostrea virginica*, *J. Exp. Biol.*, 215, 29–
988 43, <https://doi.org/10.1242/jeb.061481>, 2011.

989 Dinauer, A. and Mucci, A.: Spatial variability in surface-water pCO₂ and gas exchange in the world's largest semi-enclosed
990 estuarine system: St. Lawrence Estuary (Canada), *Biogeosciences*, 14, 3221-3237, <https://doi.org/10.5194/bg-14-3221-2017>,
991 2017.

992 Doney, S. C., Fabry, V. J., Feely, R. A., and Kleypas, J. A.: Ocean acidification: the other CO₂ problem., *Annu. Rev. Mar.*
993 *Sci.*, 1, 169–92, <https://doi.org/10.1146/annurev.marine.010908.163834>, 2009.

994 Dong, S., Lei, Y., Li, T., Cao, Y., and Xu, K.: Biocalcification crisis in the continental shelf under ocean acidification. *Geosci.*
995 *Front.*, 14(6), 101622, <https://doi.org/10.1016/j.gsf.2023.101622>, 2023.

996 Du, J., Shen, J., Park, K., Wang, Y. P., and Yu, X.: Worsened physical condition due to climate change contributes to the
997 increasing hypoxia in Chesapeake Bay, *Sci. Total Environ.*, 630, 707–717, <https://doi.org/10.1016/j.scitotenv.2018.02.265>,
998 2018.

999 Duarte, C. M., Hendriks, I. E., Moore, T. S., Olsen, Y. S., Steckbauer, A., Ramajo, L., Carstensen, J., Trotter, J. A., and
1000 McCulloch, M.: Is Ocean Acidification an Open-Ocean Syndrome? Understanding Anthropogenic Impacts on Seawater pH,
1001 *Estuaries Coasts*, 36, 221–236, <https://doi.org/10.1007/s12237-013-9594-3>, 2013.

1002 Dufresne, J.-L., Foujols, M.-A., Denvil, S., Caubel, A., Marti, O., Aumont, O., Balkanski, Y., Bekki, S., Bellenger, H.,
1003 Benshila, R., Bony, S., Bopp, L., Braconnot, P., Brockmann, P., Cadule, P., Cheruy, F., Codron, F., Cozic, A., Cugnet, D.,
1004 Noblet, N. de, Duvel, J.-P., Ethé, C., Fairhead, L., Fichefet, T., Flavoni, S., Friedlingstein, P., Grandpeix, J.-Y., Guez, L.,
1005 Guilyardi, E., Hauglustaine, D., Hourdin, F., Idelkadi, A., Ghattas, J., Joussaume, S., Kageyama, M., Krinner, G., Labetoulle,
1006 S., Lahellec, A., Lefebvre, M.-P., Lefevre, F., Levy, C., Li, Z. X., Lloyd, J., Lott, F., Madec, G., Mancip, M., Marchand, M.,
1007 Masson, S., Meurdesoif, Y., Mignot, J., Musat, I., Parouty, S., Polcher, J., Rio, C., Schulz, M., Swingedouw, D., Szopa, S.,
1008 Talandier, C., Terray, P., Viovy, N., and Vuichard, N.: Climate change projections using the IPSL-CM5 Earth System Model:
1009 from CMIP3 to CMIP5, *Clim. Dyn.*, 40, 2123–2165, <https://doi.org/10.1007/s00382-012-1636-1>, 2013.

1010 Dunne, J. P., John, J. G., Adcroft, A. J., Griffies, S. M., Hallberg, R. W., Shevliakova, E., Stouffer, R. J., Cooke, W., Dunne,
1011 K. A., Harrison, M. J., Krasting, J. P., Malyshev, S. L., Milly, P. C. D., Philipps, P. J., Sentman, L. T., Samuels, B. L., Spelman,
1012 M. J., Winton, M., Wittenberg, A. T., and Zadeh, N.: GFDL's ESM2 Global Coupled Climate–Carbon Earth System Models.

Part I: Physical Formulation and Baseline Simulation Characteristics, *J. Clim.*, 25, 6646–6665, <https://doi.org/10.1175/jcli-d-11-00560.1>, 2012.

EPA, Chesapeake Bay Total Maximum Daily Load for Nitrogen, Phosphorus, and Sediment, United States Environmental Protection Agency, 2010.

Guinotte, J. M. and Fabry, V. J.: Ocean Acidification and Its Potential Effects on Marine Ecosystems, *Ann. N. York Acad. Sci.*, 1134, 320–342, <https://doi.org/10.1196/annals.1439.013>, 2008.

Ehrich, M. K. and Harris, L. A.: A review of existing eastern oyster filtration rate models, *Ecol. Model.*, 297, 201–212, <https://doi.org/10.1016/j.ecolmodel.2014.11.023>, 2015.

Feely, R. A., Sabine, C. L., Lee, K., Berelson, W., Kleypas, J., Fabry, V. J., and Millero, F. J.: Impact of Anthropogenic CO₂ on the CaCO₃ System in the Oceans, *Science*, 305, 362–366, <https://doi.org/10.1126/science.1097329>, 2004.

Feely, R. A., Doney, S. C., and Cooley, S. R.: Ocean Acidification: Present Conditions and Future Changes in a High-CO₂ World, *Oceanography*, 22, 36–47, <https://doi.org/10.5670/oceanog.2009.95>, 2009.

Feng, Y., Friedrichs, M. A. M., Wilkin, J., Tian, H., Yang, Q., Hofmann, E. E., Wiggert, J. D., and Hood, R. R.: Chesapeake Bay nitrogen fluxes derived from a land-estuarine ocean biogeochemical modeling system: Model description, evaluation, and nitrogen budgets, *J. Geophys. Res.: Biogeosciences*, 120, 1666–1695, <https://doi.org/10.1002/2015jg002931>, 2015.

Fitzer, S. C., Torres Gabarda, S., Daly, L., Hughes, B., Dove, M., O'Connor, W., Potts, J., Scanes, P., and Byrne, M.: Coastal acidification impacts on shell mineral structure of bivalve mollusks. *Ecol. Evol.*, 8(17), 8973–8984, <https://doi.org/10.1002/ece3.4416>, 2018.

Frankel, L. T., Friedrichs, M. A. M., St-Laurent, P., Bever, A. J., Lipcius, R. N., Bhatt, G., and Shenk, G. W.: Nitrogen reductions have decreased hypoxia in the Chesapeake Bay: Evidence from empirical and numerical modeling, *Sci. Total Environ.*, 814, 152722, <https://doi.org/10.1016/j.scitotenv.2021.152722>, 2022.

Frank-Lawale, A., Allen, S. K., and Dgremont, L.: Breeding and Domestication of Eastern Oyster (*Crassostrea virginica*) Lines for Culture in the Mid-Atlantic, Usa: Line Development and Mass Selection for Disease Resistance, *J. Shellfish Res.*, 33, 153–165, <https://doi.org/10.2983/035.033.0115>, 2014.

Fujii, M., Hamanoue, R., Bernardo, L. P. C., Ono, T., Dazai, A., Oomoto, S., Wakita, M., and Tanaka, T.: Assessing impacts of coastal warming, acidification, and deoxygenation on Pacific oyster (*Crassostrea gigas*) farming: a case study in the Hinase area, Okayama Prefecture, and Shizugawa Bay, Miyagi Prefecture, Japan, *Biogeosciences*, 20, 4527–4549, <https://doi.org/10.5194/bg-20-4527-2023>, 2023.

Fulford, R., Breitburg, D., Newell, R., Kemp, W., and Luckenbach, M.: Effects of oyster population restoration strategies on phytoplankton biomass in Chesapeake Bay: a flexible modeling approach, *Mar. Ecol. Prog. Ser.*, 336, 43–61, <https://doi.org/10.3354/meps336043>, 2007.

Gattuso, Strong, A. L., Kroeker, K. J., Teneva, L. T., Mease, L. A., and Kelly, R. P.: Ocean Acidification 2.0: Managing our Changing Coastal Ocean Chemistry, *BioScience*, 64, 581–592, <https://doi.org/10.1093/biosci/biu072>, 2014.

Gawde, R. K., North, E. W., Hood, R. R., Long, W., Wang, H., and Wilberg, M. J.: A high resolution hydrodynamic-biogeochemical-oyster-filtration model predicts that the presence of oysters (*Crassostrea virginica*) can improve, or reduce, water quality depending upon oyster abundance and location. *Ecol. Model.*, 496, 110833, <https://doi.org/10.1016/j.ecolmodel.2024.110833>, 2024.

Gazeau, F., Quiblier, C., Jansen, J. M., Gattuso, J. P., Middelburg, J. J., and Heip, C. H.: Impact of elevated CO₂ on shellfish calcification. *Geophys. Res. Lett.*, 34, 7, <https://doi.org/10.1029/2006GL028554>, 2007.

Gobler, C. J. and Talmage, S. C.: Physiological response and resilience of early life-stage Eastern oysters (*Crassostrea virginica*) to past, present and future ocean acidification, *Conserv. Physiol.*, 2, cou004, <https://doi.org/10.1093/conphys/cou004>, 2014.

Goulletquer, P., Soletchnik, P., Le Moine, O., Razet, D., Geairon, P., and Faury, N.: Summer mortality of the Pacific cupped oyster *Crassostrea gigas* in the Bay of Marennes-Oléron (France), *CIEM Conseil International pour l'Exploration de la Mer*, 1998.

Gmelin, J. F.: Caroli a Linnaei Systema Naturae per Regna Tria Naturae, *Systema Naturae, Linnaeus, 13*, 3021-3910, 1791.

Gruber, N., Clement, D., Carter, B. R., Feely, R. A., Heuven, S. van, Hoppema, M., Ishii, M., Key, R. M., Kozyr, A., Lauvset, S. K., Monaco, C. L., Mathis, J. T., Murata, A., Olsen, A., Perez, F. F., Sabine, C. L., Tanhua, T., and Wanninkhof, R.: The oceanic sink for anthropogenic CO₂ from 1994 to 2007, *Science*, 363, 1193–1199, <https://doi.org/10.1126/science.aau5153>, 2019.

Guévelou, E., Carnegie, R. B., Small, J. M., Hudson, K., Reece, K. S., and Rybovich, M. M.: Tracking Triploid Mortalities of Eastern Oysters *Crassostrea virginica* in the Virginia Portion of the Chesapeake Bay, *J. Shellfish Res.*, 38, 101–113, <https://doi.org/10.2983/035.038.0110>, 2019.

Hasler, C. T., Jeffrey, J. D., Schneider, E. V. C., Hannan, K. D., Tix, J. A., and Suski, C. D.: Biological consequences of weak acidification caused by elevated carbon dioxide in freshwater ecosystems, *Hydrobiologia*, 806, 1–12, <https://doi.org/10.1007/s10750-017-3332-y>, 2018.

Herrmann, M., Najjar, R. G., Da, F., Friedman, J. R., Friedrichs, M. A. M., Goldberger, S., Menendez, A., Shadwick, E. H., Stets, E. G., and St-Laurent, P.: Challenges in Quantifying Air-Water Carbon Dioxide Flux Using Estuarine Water Quality Data: Case Study for Chesapeake Bay, *J. Geophys. Res.: Oceans*, 125, e2019JC015610, <https://doi.org/10.1029/2019jc015610>, 2020.

Hersbach, H., Bell, B., Berrisford, P., Hirahara, S., Horányi, A., Muñoz-Sabater, J., Nicolas, J., Peubey, C., Radu, R., Schepers, D., Simmons, A., Soci, C., Abdalla, S., Abellan, X., Balsamo, G., Bechtold, P., Biavati, G., Bidlot, J., Bonavita, M., Chiara, G., Dahlgren, P., Dee, D., Diamantakis, M., Dragani, R., Flemming, J., Forbes, R., Fuentes, M., Geer, A., Haimberger, L., Healy, S., Hogan, R. J., Hólm, E., Janisková, M., Keeley, S., Laloyaux, P., Lopez, P., Lupu, C., Radnoti, G., Rosnay, P., Rozum, I., Vamborg, F., Villaume, S., and Thépaut, J.: The ERA5 global reanalysis, *Q. J. R. Meteorol. Soc.*, 146, 1999–2049, <https://doi.org/10.1002/qj.3803>, 2020.

Hinson, K. E., Friedrichs, M. A. M., St-Laurent, P., Da, F., and Najjar, R. G.: Extent and Causes of Chesapeake Bay Warming, JAWRA J. Am. Water Resour. Assoc., 58, 805–825, <https://doi.org/10.1111/1752-1688.12916>, 2022.

Hinson, K. E., Friedrichs, M. A. M., Najjar, R. G., Herrmann, M., Bian, Z., Bhatt, G., St-Laurent, P., Tian, H., and Shenk, G.: Impacts and uncertainties of climate-induced changes in watershed inputs on estuarine hypoxia, Biogeosciences, 20, 1937–1961, <https://doi.org/10.5194/bg-20-1937-2023>, 2023.

[Hinson, K.E., Friedrichs, M. A. M., Najjar, R. G., Bian, Z., Herrmann, M., St-Laurent, P., 2024. Response of hypoxia to future climate change is sensitive to methodological assumptions. Scientific Reports, 14, 17544, <https://doi.org/10.1038/s41598-024-68329-3>](#)

Himes, A.R., Schatz, A. and Rivest, E.B.: Differences in larval acidification tolerance among populations of the eastern oyster, Crassostrea virginica. J. Exp. Mar. Biol. Ecol., 577, 152023, <https://doi.org/10.1016/j.jembe.2024.152023>, 2024.

Hochachka, P. W. and Somero, G. N.: Biochemical Adaptation: Mechanism and Processing Physiological Evolution. Oxford University Press, 2002.

Hofmann, G. E. and Hand, S. C.: Global arrest of translation during invertebrate quiescence., Proc. Natl. Acad. Sci., 91, 8492–8496, <https://doi.org/10.1073/pnas.91.18.8492>, 1994.

Hopkinson, C. S., Buffam, I., Hobbie, J., Vallino, J., Perdue, M., Eversmeyer, B., Prahl, F., Covert, J., Hodson, R., Moran, M. A., Smith, E., Baross, J., Crump, B., Findlay, S., and Foreman, K.: Terrestrial inputs of organic matter to coastal ecosystems: An intercomparison of chemical characteristics and bioavailability, Biogeochemistry, 43, 211–234, <https://doi.org/10.1023/a:1006016030299>, 1998.

Hudson, K.: Virginia Shellfish Aquaculture Situation and Outlook Report:Results of the 2018 Virginia Shellfish Aquaculture Crop Reporting Survey, 2019.

Intergovernmental Panel on Climate Change: IPCC Special Report on the Ocean and Cryosphere in a Changing Climate [H.-O. Pörtner, D.C. Roberts, V. Masson-Delmotte, P. Zhai, M. Tignor, E. Poloczanska, K. Mintenbeck, A. Alegria, M. Nicolai, A. Okem, J. Petzold, B. Rama, N.M. Weyer (eds.)]. Cambridge University Press, Cambridge, UK and New York, NY, USA, 755 pp. <https://doi.org/10.1017/9781009157964>, 2019.

Intergovernmental Panel on Climate Change: The Physical Science Basis, 673–816, <https://doi.org/10.1017/9781009157896.007>, 2021.

Irby, I. D., Friedrichs, M. A. M., Friedrichs, C. T., Bever, A. J., Hood, R. R., Lanerolle, L. W. J., Li, M., Linker, L., Scully, M. E., Sellner, K., Shen, J., Testa, J., Wang, H., Wang, P., and Xia, M.: Challenges associated with modeling low-oxygen waters in Chesapeake Bay: a multiple model comparison, Biogeosciences, 13, 2011–2028, <https://doi.org/10.5194/bg-13-2011-2016>, 2016.

Irby, I. D., Friedrichs, M. A. M., Da, F., and Hinson, K. E.: The competing impacts of climate change and nutrient reductions on dissolved oxygen in Chesapeake Bay, Biogeosciences, 15, 2649–2668, <https://doi.org/10.5194/bg-15-2649-2018>, 2018.

1111 Jewett, L. and Romanou, A.: Ocean acidification and other ocean changes. In: Climate Science Special Report: Fourth National
 1112 Climate Assessment, Volume I [Wuebbles, D.J., D.W. Fahey, K.A. Hibbard, D.J. Dokken, B.C. Stewart, and T.K. Maycock
 1113 (eds.)]. U.S. Global Change Research Program, Washington, DC, USA, pp. 364-392, doi: 10.7930/J0QV3JQB, 2017.
 1114 Jones, H. R., Johnson, K. M., and Kelly, M. W.: Synergistic Effects of Temperature and Salinity on the Gene Expression and
 1115 Physiology of *Crassostrea virginica*, Integr. Comp. Biol., 59, 306–319, <https://doi.org/10.1093/icb/icz035>, 2019.
 1116 Jordan, S. J.: Sedimentation and remineralization associated with biodeposition by the American oyster *Crassostrea virginica*
 1117 (Gmelin). University of Maryland, College Park, 1987.
 1118 Kellogg, M. L., Brush, M., and Cornwell, J. C.: An updated model for estimating the TMDL- related benefits of oyster reef
 1119 restoration, A final report to The Nature Conservancy and Oyster Recovery Partnership, 2018.
 1120 Kelly, C. J., Laramore, S. E., Scarpa, J., and Newell, R. I. E.: Seasonal Comparison of Physiological Adaptation and Growth
 1121 of Suminoe (*Crassostrea ariakensis*) and Eastern (*Crassostrea virginica*) Oysters, J. Shellfish Res., 30, 737–749,
 1122 <https://doi.org/10.2983/035.030.0314>, 2011.
 1123 Kemp, W., Boynton, W., Adolf, J., Boesch, D., Boicourt, W., Brush, G., Cornwell, J., Fisher, T., Glibert, P., Hagy, J., Harding,
 1124 L., Houde, E., Kimmel, D., Miller, W., Newell, R., Roman, M., Smith, E., and Stevenson, J.: Eutrophication of Chesapeake
 1125 Bay: historical trends and ecological interactions, Mar. Ecol. Prog. Ser., 303, 1–29, <https://doi.org/10.3354/meps303001>, 2005.
 1126 Kingsley-Smith, P. R., Harwell, H. D., Kellogg, M. L., Allen, S. M., Allen, S. K., Meritt, D. W., Paynter, K. T., and
 1127 Luckenbach, M. W.: Survival and Growth of Triploid *Crassostrea virginica* (Gmelin, 1791) and *C. ariakensis* (Fujita, 1913) in
 1128 Bottom Environments of Chesapeake Bay: Implications for an Introduction, J. Shellfish Res., 28, 169–184,
 1129 <https://doi.org/10.2983/035.028.0201>, 2009.
 1130 La Peyre, M.K., Eberline, B.S., Soniat, T.M. and La Peyre, J.F.: Differences in extreme low salinity timing and duration
 1131 differentially affect eastern oyster (*Crassostrea virginica*) size class growth and mortality in Breton Sound, LA, Estuar. Coast.
 1132 Shelf Sci., 135, 146-157, 2013.
 1133 Lake, S. and Brush, M.: Modeling estuarine response to load reductions in a warmer climate: York River Estuary, Virginia,
 1134 USA, Mar. Ecol. Prog. Ser., 538, 81–98, <https://doi.org/10.3354/meps11448>, 2015.
 1135 Lavaud, R., Peyre, M. K. L., Justic, D., and Peyre, J. F. L.: Dynamic Energy Budget modelling to predict eastern oyster growth,
 1136 reproduction, and mortality under river management and climate change scenarios, Estuar., Coast. Shelf Sci., 251, 107188,
 1137 <https://doi.org/10.1016/j.ecss.2021.107188>, 2021.
 1138 Lavaud, R., Peyre, M. K. L., Couvillion, B., Pollack, J. B., Brown, V., Palmer, T. A., and Keim, B.: Predicting restoration and
 1139 aquaculture potential of eastern oysters through an eco-physiological mechanistic model, Ecol. Model., 489, 110603,
 1140 <https://doi.org/10.1016/j.ecolmodel.2023.110603>, 2024.
 1141 Lemasson, A. J., Hall-Spencer, J. M., Fletcher, S., Provstgaard-Morys, S., and Knights, A. M.: Indications of future
 1142 performance of native and non-native adult oysters under acidification and warming, Mar. Environ. Res., 142, 178–189,
 1143 <https://doi.org/10.1016/j.marenvres.2018.10.003>, 2018.

Li, M., Lee, Y. J., Testa, J. M., Li, Y., Ni, W., Kemp, W. M., and Toro, D. M. D.: What drives interannual variability of hypoxia in Chesapeake Bay: Climate forcing versus nutrient loading?, *Geophys. Res. Lett.*, 43, 2127–2134, <https://doi.org/10.1002/2015gl067334>, 2016.

Liddel, M. K.: A von Bertalanffy based model for the estimation of oyster (*Crassostrea virginica*) growth on restored oyster reefs in Chesapeake Bay, 2008.

Liu, Z., Zhou, Z., Zhang, Y., Wang, L., Song, X., Wang, W., Zheng, Y., Zong, Y., Lv, Z., and Song, L.: Ocean acidification inhibits initial shell formation of oyster larvae by suppressing the biosynthesis of serotonin and dopamine. *Sci. Total Environ.*, 735, 139469, <https://doi.org/10.1016/j.scitotenv.2020.139469>, 2020.

Loosanoff, V. L.: Some aspects of behavior of oysters at different temperatures, *Biol. Bull.*, 114, 57–70, <https://doi.org/10.2307/1538965>, 1958.

López-Urrutia, Á., Martin, E. S., Harris, R. P., and Irigoien, X.: Scaling the metabolic balance of the oceans, *Proc. Natl. Acad. Sci.*, 103, 8739–8744, <https://doi.org/10.1073/pnas.0601137103>, 2006.

Lowe, A. T., Kobelt, J., Horwith, M., and Ruesink, J.: Ability of Eelgrass to Alter Oyster Growth and Physiology Is Spatially Limited and Offset by Increasing Predation Risk, *Estuaries Coasts*, 42, 743–754, <https://doi.org/10.1007/s12237-018-00488-9>, 2019.

Lutier, M., Di Poi, C., Gazeau, F., Appolis, A., Le Luyet, J., and Pernet, F.: Revisiting tolerance to ocean acidification: insights from a new framework combining physiological and molecular tipping points of Pacific oyster. *Glob. Change Bio.*, 28(10), 3333–3348, <https://doi.org/10.1111/gcb.16101>, 2022.

Mazarrasa, I., Marbà, N., Lovelock, C. E., Serrano, O., Lavery, P. S., Fourqurean, J. W., Kennedy, H., Mateo, M. A., Krause-Jensen, D., Steven, A. D. L., and Duarte, C. M.: Seagrass meadows as a globally significant carbonate reservoir, *Biogeosciences*, 12, 4993–5003, <https://doi.org/10.5194/bg-12-4993-2015>, 2015.

Matoo, O. B., Lannig, G., Bock, C., and Sokolova, I. M.: Temperature but not ocean acidification affects energy metabolism and enzyme activities in the blue mussel, *Mytilus edulis*. *Ecol. Evol.*, 11(7), 3366–3379, <https://doi.org/10.1002/ece3.7289>, 2021.

Medeiros, I. P. M., and Souza, M. M.: Acid times in physiology: a systematic review of the effects of ocean acidification on calcifying invertebrates. *Environmental Research*, 116019, <https://doi.org/10.1016/j.envres.2023.116019>, 2023.

Melzner, F., Mark, F.C., Seibel, B.A. and Tomanek, L.: Ocean acidification and coastal marine invertebrates: tracking CO₂ effects from seawater to the cell. *Annu. Rev. Mar. Sci.*, 12, pp.499–523, <https://doi.org/10.1146/annurev-marine-010419-010658>, 2020.

Mitchell, M., Herman, J., Bilkovic, D. M., and Hershner, C.: Marsh persistence under sea-level rise is controlled by multiple, geologically variable stressors, *Ecosyst. Heal. Sustain.*, 3, 1379888, <https://doi.org/10.1080/20964129.2017.1396009>, 2017.

Mizuta, D. D., Silveira, N., Fischer, C. E., and Lemos, D.: Interannual variation in commercial oyster (*Crassostrea gigas*) farming in the sea (Florianópolis, Brazil, 27°44' S; 48°33' W) in relation to temperature, chlorophyll a and associated oceanographic conditions, *Aquaculture*, 366, 105–114, <https://doi.org/10.1016/j.aquaculture.2012.09.011>, 2012.

1178 Mizuta, D. D. and Wikfors, G. H.: Seeking the perfect oyster shell: a brief review of current knowledge, *Rev. Aquac.*, 11, 586–
1179 602, <https://doi.org/10.1111/raq.12247>, 2019.

1180 Moore, K. A., Orth, R. J., and Wilcox, D. J.: Assessment of the Abundance of Submersed Aquatic Vegetation (SAV)
1181 Communities in the Chesapeake Bay and its Use in SAV Management, in: *Remote Sensing and Geospatial Technologies for*
1182 *Coastal Ecosystem Assessment and Management*, <https://doi.org/10.1007/978-3-540-88183-4>, 2009.

1183 Moore-Maley, B. L., Allen, S. E., and Ianson, D.: Locally driven interannual variability of near-surface pH and Ω_A in the
1184 Strait of Georgia, *J. Geophys. Res.: Oceans*, 121, 1600–1625, <https://doi.org/10.1002/2015jc011118>, 2016.

1185 Moriarty, J. M., Friedrichs, M. A. M., and Harris, C. K.: Seabed Resuspension in the Chesapeake Bay: Implications for
1186 Biogeochemical Cycling and Hypoxia, *Estuaries Coasts*, 44, 103–122, <https://doi.org/10.1007/s12237-020-00763-8>, 2021.

1187 Najjar, R. G., Herrmann, M., Valle, S. M. C. D., Friedman, J. R., Friedrichs, M. A. M., Harris, L. A., Shadwick, E. H., Stets,
1188 E. G., and Woodland, R. J.: Alkalinity in Tidal Tributaries of the Chesapeake Bay, *J. Geophys. Res.: Oceans*, 125,
1189 <https://doi.org/10.1029/2019jc015597>, 2020.

1190 Newell, R. I. E. and Koch, E. W.: Modeling seagrass density and distribution in response to changes in turbidity stemming
1191 from bivalve filtration and seagrass sediment stabilization, *Estuaries*, 27, 793–806, <https://doi.org/10.1007/bf02912041>, 2004.

1192 Ni, W., Li, M., and Testa, J. M.: Discerning effects of warming, sea level rise and nutrient management on long-term hypoxia
1193 trends in Chesapeake Bay, *Sci. Total Environ.*, 737, 139717, <https://doi.org/10.1016/j.scitotenv.2020.139717>, 2020.

1194 Olson, M.: *Guide to Using Chesapeake Bay Program Water Quality Monitoring Data*, Chesapeake Bay Program, Annapolis,
1195 MD, 2012.

1196 Nichols, M.M., Kim, S.C. and Brouwer, C.M.: *Sediment Characterization of Chesapeake Bay and Its Tributaries*, 1991.

1197 Orr, J.C., Fabry, V.J., Aumont, O., Bopp, L., Doney, S.C., Feely, R.A., Gnanadesikan, A., Gruber, N., Ishida, A., Joos, F. and
1198 Key, R.M.: Anthropogenic ocean acidification over the twenty-first century and its impact on calcifying organisms,
1199 *Nature*, 437, 681–686, <https://doi.org/10.1038/nature04095>, 2005.

1200 Orth, R. J., Nowak, J. F., Wilcox, D. J., Whiting, J. R., and Nagey, L. S.: Distribution of Submerged Aquatic Vegetation in the
1201 Chesapeake Bay and Tributaries and the Coastal Bays, *Am. Zoöl.*, 3, 315–317, <https://doi.org/10.1093/icb/3.3.315>, 1998.

1202 Pacella, S.R., Brown, C.A., Kaldy, J.E., Labiosa, R.G., Hales, B., Mochon Collura, T.C. and Waldbusser, G.G.: Quantifying
1203 the combined impacts of anthropogenic CO₂ emissions and watershed alteration on estuary acidification at biologically-
1204 relevant time scales: a case study from Tillamook Bay, OR, USA. *Front. Mar. Sci.*, 11, 1293955,
1205 <https://doi.org/10.3389/fmars.2024.1293955>, 2024.

1206 Palmer, S. C. J., Gernez, P. M., Thomas, Y., Simis, S., Miller, P. I., Glize, P., and Barillé, L.: Remote Sensing-Driven Pacific
1207 Oyster (*Crassostrea gigas*) Growth Modeling to Inform Offshore Aquaculture Site Selection, *Front. Mar. Sci.*, 6, 802,
1208 <https://doi.org/10.3389/fmars.2019.00802>, 2020.

1209 Palmer, S. C. J., Barillé, L., Kay, S., Ciavatta, S., Buck, B., and Gernez, P.: Pacific oyster (*Crassostrea gigas*) growth modelling
1210 and indicators for offshore aquaculture in Europe under climate change uncertainty, *Aquaculture*, 532, 736116,
1211 <https://doi.org/10.1016/j.aquaculture.2020.736116>, 2021.

Paynter, K. T., Goodwin, J. D., Chen, M. E., Ward, N. J., Sherman, M. W., Meritt, D. W., and Allen, S. K.: *Crassostrea ariakensis* in Chesapeake Bay: Growth, Disease and Mortality in Shallow Subtidal Environments, *J. Shellfish Res.*, 27, 509–515, [https://doi.org/10.2983/0730-8000\(2008\)27\[509:caicbg\]2.0.co;2](https://doi.org/10.2983/0730-8000(2008)27[509:caicbg]2.0.co;2), 2008.

Peyre, M. K. L., Eberline, B. S., Soniat, T. M., and Peyre, J. F. L.: Differences in extreme low salinity timing and duration differentially affect eastern oyster (*Crassostrea virginica*) size class growth and mortality in Breton Sound, LA, *Estuar., Coast. Shelf Sci.*, 135, 146–157, <https://doi.org/10.1016/j.ecss.2013.10.001>, 2013.

Planton, S., Déqué, M., Chauvin, F., and Terray, L.: Expected impacts of climate change on extreme climate events, *C. R. Geosci.*, 340, 564–574, <https://doi.org/10.1016/j.crte.2008.07.009>, 2008.

Poach, M., Munroe, D., Vasslides, J., Abrahamsen, I. and Coffey, N.: Monitoring coastal acidification along the US East coast: concerns for shellfish production. *Bull. Jap. Fish. Res. Edu. Agen. No.*, 49, 53-64, 2019.

Ramajo, L., Pérez-León, E., Hendriks, I. E., Marbà, N., Krause-Jensen, D., Sejr, M. K., Blicher, M. E., Lagos, N. A., Olsen, Y. S., and Duarte, C. M.: Food supply confers calcifiers resistance to ocean acidification, *Sci. Rep.*, 6, 19374, <https://doi.org/10.1038/srep19374>, 2016.

Raymond, P. A., Bauer, J. E., and Cole, J. J.: Atmospheric CO₂ evasion, dissolved inorganic carbon production, and net heterotrophy in the York River estuary, *Limnol. Oceanogr.*, 45, 1707–1717, <https://doi.org/10.4319/lo.2000.45.8.1707>, 2000.

Riahi, K., Rao, S., Krey, V., Cho, C., Chirkov, V., Fischer, G., Kindermann, G., Nakicenovic, N., and Rafaj, P.: RCP 8.5—A scenario of comparatively high greenhouse gas emissions, *Clim. Chang.*, 109, 33, <https://doi.org/10.1007/s10584-011-0149-y>, 2011.

Redfield, A.C.: On the proportions of organic derivatives in sea water and their relation to the composition of plankton, University Press of Liverpool, Liverpool, UK, 1934.

Reid, J.M., Reid, J.A., Jenkins, C.J., Hastings, M.E., Williams, S.J. and Poppe, L.J.: usSEABED: Atlantic coast offshore surficial sediment data release, US Geological Survey Data Series, 118, 2005.

Rivest, E.B., Brush, M., Zimmerman, R., Hill, V.,” Can Meadows of Submerged Aquatic Vegetation (SAV) Mitigate Ocean Acidification Thresholds for Eastern Oysters in the Chesapeake Bay? Final report, NOAA Ocean Acidification Program. Award number NA18NOS4780177, 2023.

Roden, E. and Tuttle, J.: Inorganic sulfur cycling in mid and lower Chesapeake Bay sediments, *Mar. Ecol. Prog. Ser.*, 93, 101–118, <https://doi.org/10.3354/meps093101>, 1993.

Rybovich, M., Peyre, M. K. L., Hall, S. G., and Peyre, J. F. L.: Increased Temperatures Combined with Lowered Salinities Differentially Impact Oyster Size Class Growth and Mortality, *J. Shellfish Res.*, 35, 101–113, <https://doi.org/10.2983/035.035.0112>, 2016.

Saavedra, L., Bastías, M., Mendoza, P., Lagos, N. A., García-Herrera, C., Ponce, V., Alvarez, F., and Llanos-Rivera, A.: Environmental correlates of oyster farming in an upwelling system: Implication upon growth, biomass production, shell strength and organic composition, *Mar. Environ. Res.*, <https://doi.org/10.1016/j.marenvres.2024.106489>, 2024.

Deleted: . ,

1246 Salisbury, J., Green, M., Hunt, C., and Campbell, J.: Coastal Acidification by Rivers: A Threat to Shellfish?, *Eos, Trans. Am.*
 1247 *Geophys. Union*, 89, 513–513, <https://doi.org/10.1029/2008eo500001>, 2008.
 1248 Schwaner, C., Barbosa, M., Schwemmer, T. G., Espinosa, E. P., and Allam, B.: Increased Food Resources Help Eastern Oyster
 1249 Mitigate the Negative Impacts of Coastal Acidification, *Animals*, 13, 1161, <https://doi.org/10.3390/ani13071161>, 2023.
 1250 Simone, M. N., Schulz, K. G., Oakes, J. M., and Eyre, B. D.: Warming and ocean acidification may decrease estuarine
 1251 dissolved organic carbon export to the ocean, *Biogeosciences*, 18, 1823–1838, <https://doi.org/10.5194/bg-18-1823-2021>, 2021.
 1252 Nixon, S.W.: Coastal marine eutrophication: A definition, social causes, and future concerns, *Ophelia*, 41, 199–219,
 1253 <https://doi.org/10.1080/00785236.1995.10422044>, 1995.
 1254 Shadwick, E. H., Friedrichs, M. A. M., Najjar, R. G., Meo, O. A. D., Friedman, J. R., Da, F., and Reay, W. G.: High-Frequency
 1255 CO₂ System Variability Over the Winter-to-Spring Transition in a Coastal Plain Estuary, *J. Geophys. Res.: Oceans*, 124, 7626–
 1256 7642, <https://doi.org/10.1029/2019jc015246>, 2019.
 1257 Shchepetkin, A. F. and McWilliams, J. C.: The regional oceanic modeling system (ROMS): a split-explicit, free-surface,
 1258 topography-following-coordinate oceanic model, *Ocean Model.*, 9, 347–404, <https://doi.org/10.1016/j.ocemod.2004.08.002>,
 1259 2005.
 1260 Shen, C., Testa, J. M., Li, M., Cai, W., Waldbusser, G. G., Ni, W., Kemp, W. M., Cornwell, J., Chen, B., Brodeur, J., and Su,
 1261 J.: Controls on Carbonate System Dynamics in a Coastal Plain Estuary: A Modeling Study, *J. Geophys. Res.: Biogeosciences*,
 1262 124, 61–78, <https://doi.org/10.1029/2018jg004802>, 2019a.
 1263 Shen, C., Testa, J. M., Ni, W., Cai, W., Li, M., and Kemp, W. M.: Ecosystem Metabolism and Carbon Balance in Chesapeake
 1264 Bay: A 30-Year Analysis Using a Coupled Hydrodynamic-Biogeochemical Model, *J. Geophys. Res.: Oceans*, 124, 6141–
 1265 6153, <https://doi.org/10.1029/2019jc015296>, 2019b.
 1266 Shen, C., Testa, J. M., Li, M., and Cai, W.: Understanding Anthropogenic Impacts on pH and Aragonite Saturation State in
 1267 Chesapeake Bay: Insights From a 30-Year Model Study, *J. Geophys. Res.: Biogeosciences*, 125,
 1268 <https://doi.org/10.1029/2019jg005620>, 2020.
 1269 Siedlecki, S. A., Pilcher, D., Howard, E. M., Deutsch, C., MacCready, P., Norton, E. L., Frenzel, H., Newton, J., Feely, R. A.,
 1270 Alin, S. R., and Klinger, T.: Coastal processes modify projections of some climate-driven stressors in the California Current
 1271 System, *Biogeosciences*, 18, 2871–2890, <https://doi.org/10.5194/bg-18-2871-2021>, 2021a.
 1272 Siedlecki, S., Salisbury, J., Gledhill, D., Bastidas, C., Meseck, S., McGarry, K., Hunt, C., Alexander, M., Lavoie, D., Wang,
 1273 Z., Scott, J., Brady, D., Mlsna, I., Azetsu-Scott, K., Liberti, C., Melrose, D., White, M., Pershing, A., Vandemark, D.,
 1274 Townsend, D., Chen, C., Mook, W., and Morrison, R.: Projecting ocean acidification impacts for the Gulf of Maine to 2050,
 1275 *Elem.: Sci. Anthr.*, 9, <https://doi.org/10.1525/elementa.2020.00062>, 2021b.
 1276 Speights, C. J., Silliman, B. R., and McCoy, M. W.: The effects of elevated temperature and dissolved pCO₂ on a marine
 1277 foundation species, *Ecol. Evol.*, 7, 3808–3814, <https://doi.org/10.1002/ece3.2969>, 2017.

1278 Simpson, E., Ianson, D., Kohfeld, K. E., Franco, A. C., Covert, P. A., Davelaar, M., and Perreault, Y.: Variability and drivers
1279 of carbonate chemistry at shellfish aquaculture sites in the Salish Sea, British Columbia. *Biogeosciences*, 21, 1323-1353,
1280 <https://doi.org/10.5194/bg-21-1323-2024>, 2024.

1281 Stevens, A. and Gobler, C.: Interactive effects of acidification, hypoxia, and thermal stress on growth, respiration, and survival
1282 of four North Atlantic bivalves, *Mar. Ecol. Prog. Ser.*, 604, 143–161, <https://doi.org/10.3354/meps12725>, 2018.

1283 St-Laurent, P. and Friedrichs, M. A. M.: On the Sensitivity of Coastal Hypoxia to Its External Physical Forcings, *J. Adv.*
1284 *Model. Earth Syst.*, 16, <https://doi.org/10.1029/2023ms003845>, 2024.

1285 St-Laurent, P., Friedrichs, M. A. M., Najjar, R. G., Shadwick, E. H., Tian, H., and Yao, Y.: Relative impacts of global changes
1286 and regional watershed changes on the inorganic carbon balance of the Chesapeake Bay, *Biogeosciences*, 17, 3779–3796,
1287 <https://doi.org/10.5194/bg-17-3779-2020>, 2020.

1288 Su, J., Cai, W.-J., Brodeur, J., Chen, B., Hussain, N., Yao, Y., Ni, C., Testa, J. M., Li, M., Xie, X., Ni, W., Scaboo, K. M., Xu,
1289 Y., Cornwell, J., Gurbisz, C., Owens, M. S., Waldbusser, G. G., Dai, M., and Kemp, W. M.: Chesapeake Bay acidification
1290 buffered by spatially decoupled carbonate mineral cycling, *Nat. Geosci.*, 13, 441–447, [https://doi.org/10.1038/s41561-020-](https://doi.org/10.1038/s41561-020-0584-3)
1291 0584-3, 2020.

1292 Swam, L. M., Couvillion, B., Callam, B., Peyre, J. F. L., and Peyre, M. K. L.: Defining oyster resource zones across coastal
1293 Louisiana for restoration and aquaculture, *Ocean Coast. Manag.*, 225, 106178,
1294 <https://doi.org/10.1016/j.ocecoaman.2022.106178>, 2022.

1295 Talmage, S. C. and Gobler, C. J.: Effects of Elevated Temperature and Carbon Dioxide on the Growth and Survival of Larvae
1296 and Juveniles of Three Species of Northwest Atlantic Bivalves, *PLoS ONE*, 6, e26941,
1297 <https://doi.org/10.1371/journal.pone.0026941>, 2011.

1298 Tian, R., Cerco, C. F., Bhatt, G., Linker, L. C., and Shenk, G. W.: Mechanisms Controlling Climate Warming Impact on the
1299 Occurrence of Hypoxia in Chesapeake Bay, *JAWRA J. Am. Water Resour. Assoc.*, 58, 855–875, [https://doi.org/10.1111/1752-](https://doi.org/10.1111/1752-1688.12907)
1300 1688.12907, 2022.

1301 Thomsen, J., Haynert, K., Wegner, K. M., and Melzner, F.: Impact of seawater carbonate chemistry on the calcification of
1302 marine bivalves, *Biogeosciences*, 12, 4209–4220, <https://doi.org/10.5194/bg-12-4209-2015>, 2015.

1303 Turner, J. S., St-Laurent, P., Friedrichs, M. A. M., and Friedrichs, C. T.: Effects of reduced shoreline erosion on Chesapeake
1304 Bay water clarity, *Sci. Total Environ.*, 769, 145157, <https://doi.org/10.1016/j.scitotenv.2021.145157>, 2021.

1305 [USDA National Agricultural Statistics Service, 2023 Census of Aquaculture, 2023.](#)

1306 van Heuven, S., D. Pierrot, J.W.B. Lewis, R.E., and Wallace, D.W.R.: MATLAB Program Developed for CO₂ System
1307 Calculations. ORNL/CDIAC-105b. Carbon Dioxide Information Analysis Center, Oak Ridge National Laboratory, U.S.
1308 Department of Energy, Oak Ridge, Tennessee. https://doi.org/10.3334/CDIAC/otg.CO2SYS_MATLAB_v1.1, 2011.

1309 VOSARA: <https://cmap22.vims.edu/VOSARA/>, last access: 28 January 2024.

1310 Waldbusser, G. G., Voigt, E. P., Bergschneider, H., Green, M. A., and Newell, R. I. E.: Biocalcification in the Eastern Oyster
1311 (*Crassostrea virginica*) in Relation to Long-term Trends in Chesapeake Bay pH, *Estuaries Coasts*, 34, 221–231,
1312 <https://doi.org/10.1007/s12237-010-9307-0>, 2011.

1313 Wallace, R. B., Baumann, H., Grear, J. S., Aller, R. C., and Gobler, C. J.: Coastal ocean acidification: The other eutrophication
1314 problem, *Estuar., Coast. Shelf Sci.*, 148, 1–13, <https://doi.org/10.1016/j.ecss.2014.05.027>, 2014.

1315 Warner, J. C., Defne, Z., Haas, K., and Arango, H. G.: A wetting and drying scheme for ROMS, *Comput. Geosci.*, 58, 54–61,
1316 <https://doi.org/10.1016/j.cageo.2013.05.004>, 2013.

1317 Zhang, Q., Fisher, T. R., Trentacoste, E. M., Buchanan, C., Gustafson, A. B., Karrh, R., Murphy, R. R., Keisman, J., Wu, C.,
1318 Tian, R., Testa, J. M., and Tango, P. J.: Nutrient limitation of phytoplankton in Chesapeake Bay: Development of an empirical
1319 approach for water-quality management, *Water Res.*, 188, 116407, <https://doi.org/10.1016/j.watres.2020.116407>, 2021.

1320

1321 [Table 1](#). Experimental design for future simulations conducted for comparison to reference run. Model forcings include a
1322 combination of 2017 (reference) and 2067 (future) inputs of atmospheric CO₂, atmospheric temperature, and terrestrial nutrient
1323 loadings.

Future Simulation Name	Atmospheric CO ₂	Atmospheric Temperature	Terrestrial inputs
Combined Future	Future	Future	TMDL ^a
AtmCO ₂	Future	Reference	Reference
Temp	Reference	Future	Reference
TMDL	Reference	Reference	TMDL
AtmCO ₂ + Temp	Future	Future	Reference

1324 ^aTMDL (Total Maximum Daily Load) forcing includes inputs of nitrate, ammonium, and dissolved and particulate organic
1325 matter under the assumption that the nutrient reduction goals (EPA, 2010) are met.

Moved (insertion) [8]

Deleted:
Captions:

 Table 1. Model skill statistics (mean ± standard deviation) comparing bottom grid cells from the reference run to Chesapeake Bay Program observations from the same station location and time, within the bottom 10% of the water column.

 Table 2.

Formatted: Font: +Body (Times New Roman)

Formatted: Normal, Line spacing: single

Formatted: Subscript



1335 Table 2. Model skill statistics (mean ± standard deviation) comparing bottom grid cells from the reference run to Chesapeake
1336 Bay Program observations from the same station location and time, within the bottom 10% of the water column.

Variable	Model	Observation	Model Bias	RMSD ^a
Temperature (°C) n = 130	17.0 ± 9	16.7 ± 9	+ 0.2	0.7
Salinity n = 127	13.9 ± 7	15.4 ± 7	-1.5	2.7
Oxygen (mg O ₂ L ⁻¹) n = 130	8.0 ± 2.3	7.2 ± 2.9	+0.9	1.3
pH n = 74	7.8 ± 0.4	7.6 ± 0.4	+ 0.2	0.4
TSS (mg L ⁻¹) n = 74	44 ± 34	45 ± 54	-1.1	48.3
POC (g C m ⁻³) n = 74	0.7 ± 0.3	1.7 ± 2.1	-1.0	2.4

1337 ^aRMSD = root mean squared difference

Moved (insertion) [10]

Moved (insertion) [9]

Deleted: 
Table 3. Bottom environmental variables for each model simulation (annual mean ± standard deviation) for grid cells that support oyster growth in the reference run (defined as those with greater than 1g dry tissue weight after one year of growth; Fig. S2). Analogous results averaged over all model grid cells are shown in Table S5.

Formatted: Font: +Body (Times New Roman)

Formatted: Font: +Body (Times New Roman)

Formatted: Normal, Line spacing: single

1345 Table 3. Bottom environmental variables for each model simulation (annual mean ± standard deviation) for grid cells that
1346 support oyster growth in the reference run (defined as those with greater than 1g dry tissue weight after one year of growth;
1347 Fig. S2). Analogous results averaged over all model grid cells are shown in Table S5.

Model Simulation	Temperature (°C)	Salinity	POC (g C m ⁻³)	Ω _{Ca}	Dissolved Oxygen (mg O ₂ L ⁻¹)	TSS (mg L ⁻¹)
Reference	17.0 ± 0.7	15.7 ± 2.1	1.12 ± 0.1	2.5 ± 0.49	9.1 ± 0.6	11.4 ± 5.8
Combined Future	18.5 ± 0.8	16.0 ± 2.1	1.03 ± 0.1	1.6 ± 0.35	8.7 ± 0.6	11.1 ± 5.9
AtmCO ₂	17.0 ± 0.7	15.7 ± 2.1	1.12 ± 0.1	1.6 ± 0.35	9.1 ± 0.6	11.4 ± 5.8
Temp	18.5 ± 0.8	16.0 ± 2.1	1.07 ± 0.1	2.5 ± 0.41	8.8 ± 0.6	11.1 ± 5.9
TMDL	17.0 ± 0.7	15.7 ± 2.1	1.08 ± 0.1	2.4 ± 0.53	9.1 ± 0.6	11.2 ± 5.9
Temp + CO ₂	18.5 ± 0.8	16.0 ± 2.1	1.07 ± 0.1	1.7 ± 0.33	8.8 ± 0.6	11.1 ± 5.9

Moved (insertion) [11]

Formatted: Font: +Body (Times New Roman)





Formatted: Left

1348

1349 Table 4. Modeled oyster characteristics from the end of each simulation (mean ± standard deviation) over grid cells that support
1350 oyster growth in the reference run (defined as those with greater than 1g dry tissue weight after one year of growth; Fig. S2).

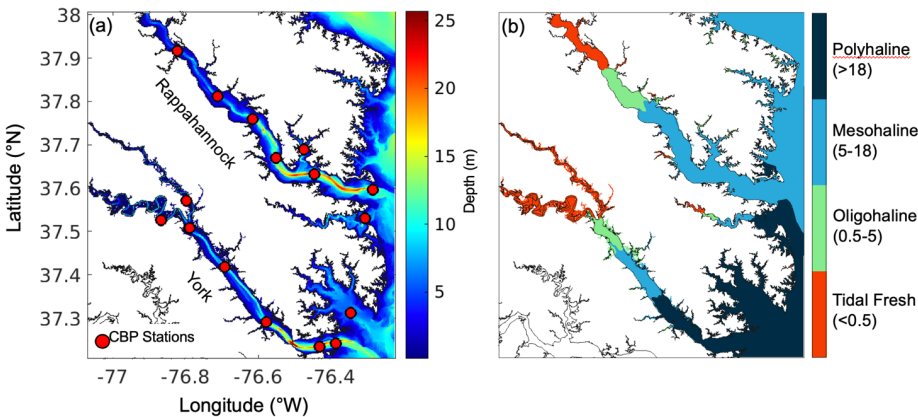
Model Simulation	Shell Weight (g)	Tissue Weight (g)	Shell Thickness (g mm ⁻¹)
Reference	16.8 ± 10.9	2.2 ± 1.5	0.18 ± 0.08
Combined Future	5.4 ± 5.7	0.9 ± 0.8	0.07 ± 0.05
AtmCO ₂	10.5 ± 8.0	2.2 ± 1.5	0.12 ± 0.06
Temp	9.7 ± 9.1	1.2 ± 1.1	0.10 ± 0.07
TMDL	13.1 ± 8.2	1.7 ± 1.2	0.15 ± 0.06
Temp + CO ₂	6.6 ± 7.1	1.2 ± 1.1	0.08 ± 0.06

Formatted: Font: +Body (Times New Roman)

Deleted: 
Figure 1. ROMS-ECBO model domain of Chesapeake Bay tributaries illustrating (a) bathymetry in meters and locations of Chesapeake Bay Program (CBP) water quality monitoring stations (red circles) and (b) bottom salinity zones. 
 Figure 2. 

1351

1359



1360

1361 Figure 1. ROMS-ECBO model domain of Chesapeake Bay tributaries illustrating (a) bathymetry in meters and locations of
1362 Chesapeake Bay Program (CBP) water quality monitoring stations (red circles) and (b) bottom salinity zones.

Moved (insertion) [12]

Formatted: Space After: 10 pt, Line spacing: single

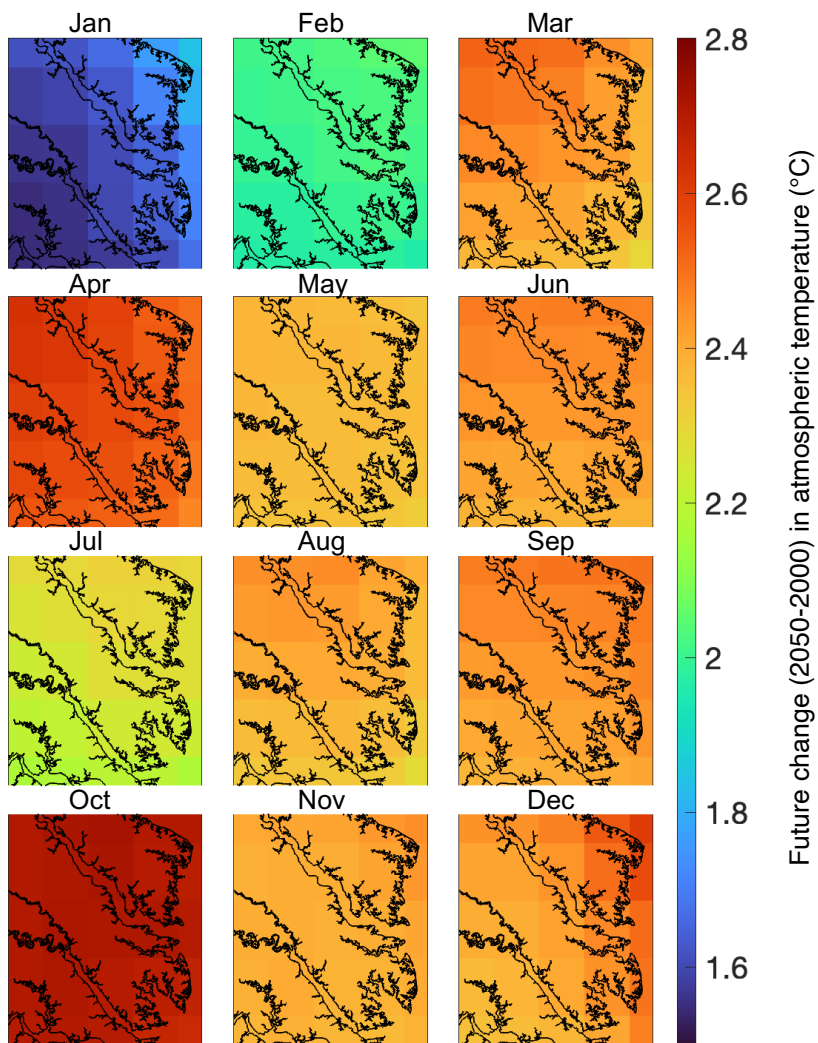


Figure 2. Monthly-averaged 50-year atmospheric temperature differences over the ROMS-ECBO model domain calculated as projections from 2050 minus those from 2000.

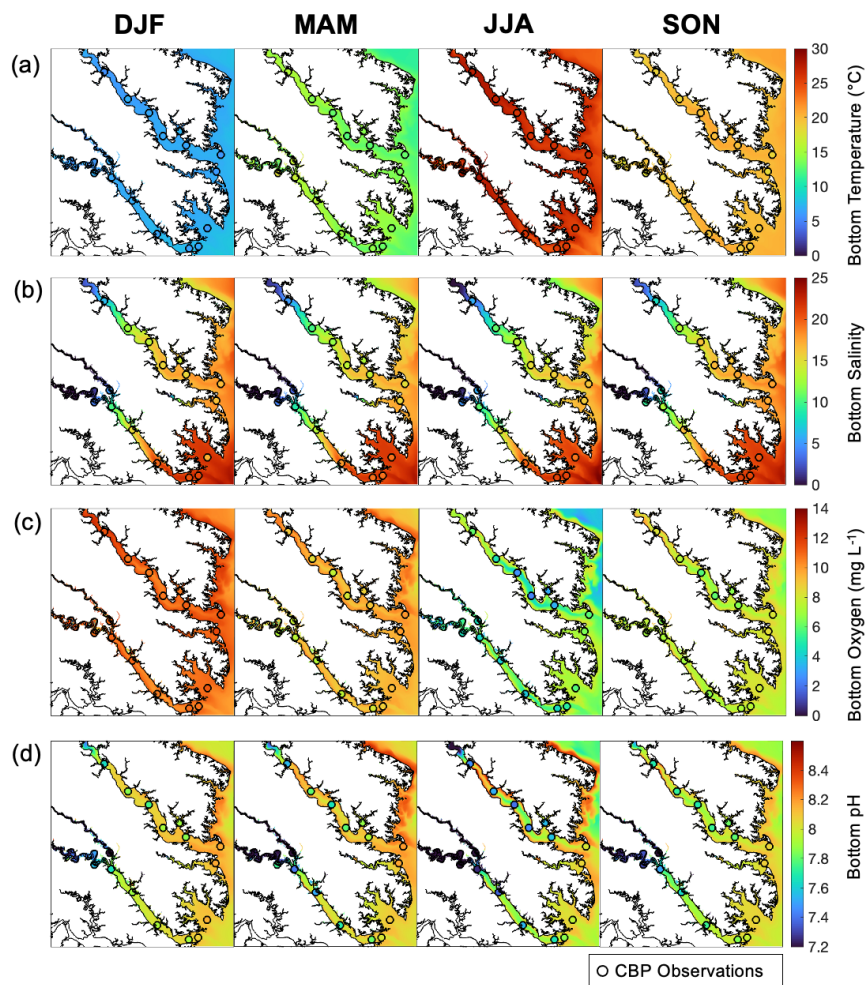


Figure 3. Seasonally-averaged bottom (a) temperature, (b) salinity, (c) dissolved oxygen, and (d) pH from the reference run. Circles represent seasonal decadal-averaged *in situ* observations at Chesapeake Bay Program stations (2010-2020). (DJF = winter, MAM = spring, JJA = summer, and SON = fall).

Formatted: Normal, Line spacing: single

Deleted: Figure 1 ROMS-ECBO model domain of Chesapeake Bay tributaries illustrating (a) bathymetry in meters and locations of Chesapeake Bay Program water quality monitoring stations (red circles) and (b) bottom salinity zones.

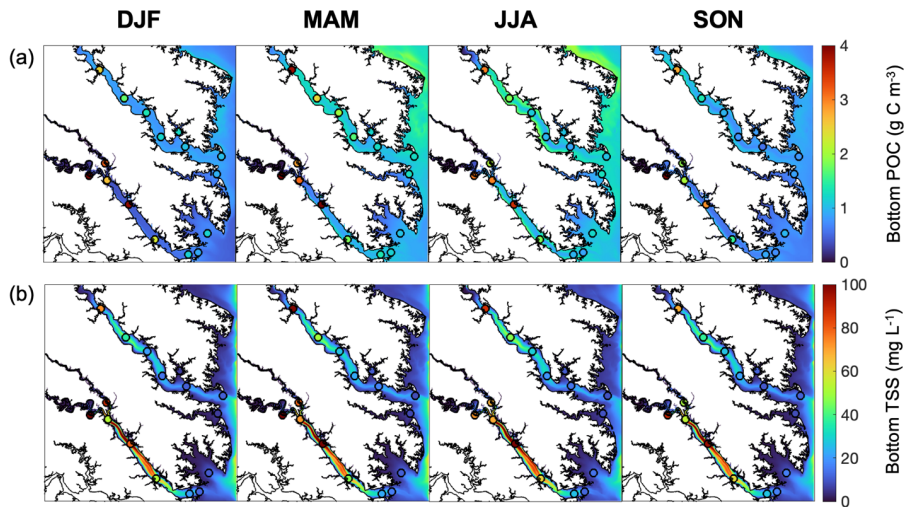


Figure 4. Seasonally-averaged bottom (a) POC and (b) TSS from output of the reference run of the ROMS-ECBO model. Circles represent seasonal decadal-averaged bottom measurements at Chesapeake Bay Program stations (2010-2020). (DJF = winter, MAM = spring, JJA = summer, and SON = fall).

Moved (insertion) [13]

Deleted:

Figure 3. Seasonally-averaged bottom (a) POC and (b) TSS from output of the reference run of the ROMS-ECBO model. Circles represent seasonal decadal-averaged bottom measurements at Chesapeake Bay Program stations (2010-2020). (DJF = winter, MAM = spring, JJA = summer, and SON = fall).

Figure 4. Monthly-averaged 50-year atmospheric temperature differences over the ROMS-ECBO model domain calculated as projections from 2050 minus those from 2000.

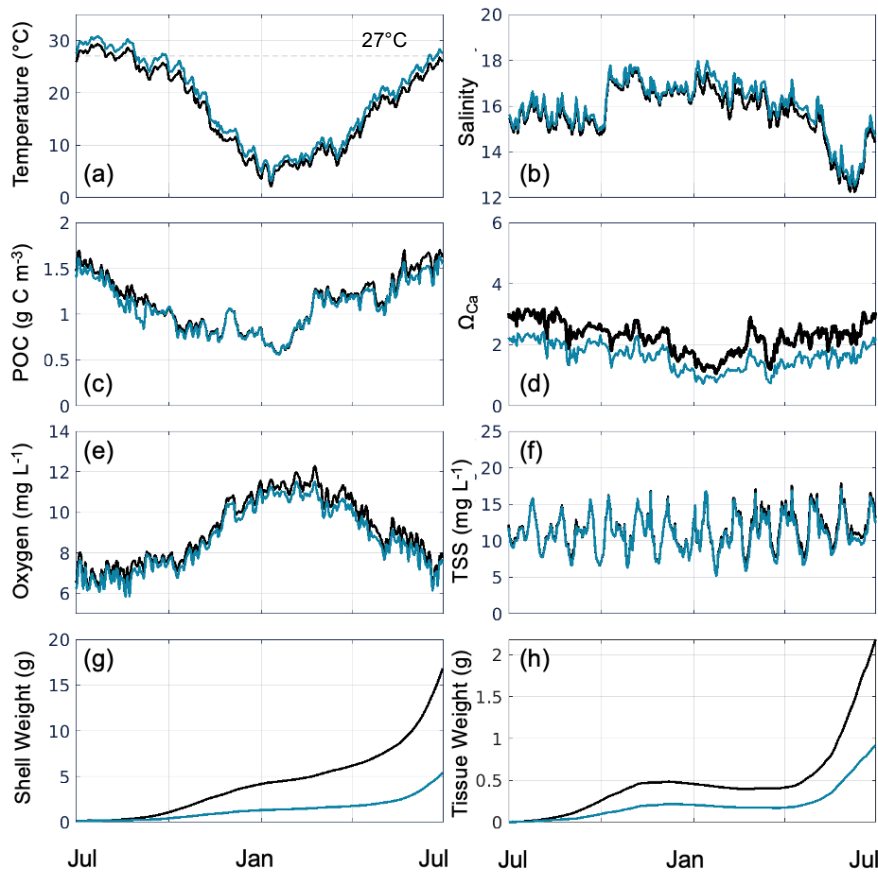


Figure 5. Time series of daily bottom (a) temperature, (b) salinity, (c) POC, (d) Ω_{Ca} , (e) oxygen, (f) TSS, (g) shell weight, and (h) tissue weight, averaged over grid cells that support oyster growth in the reference run, for the present-day reference run (black line) and Combined Future simulation (blue line). The horizontal dashed line in (a) represents the optimal filtration temperature in EcoOyster (27°C).

Formatted: Space After: 10 pt, Line spacing: single

Deleted: f

Deleted: 1

Figure 6. Annual mean bottom

Deleted: -c) POC and (d-f) Ω_{Ca} from (a,d) the present-day reference run, (b,e) the Combined Future simulation, and (c,f) the difference between (a) and (b), i.e., Combined Future minus reference.

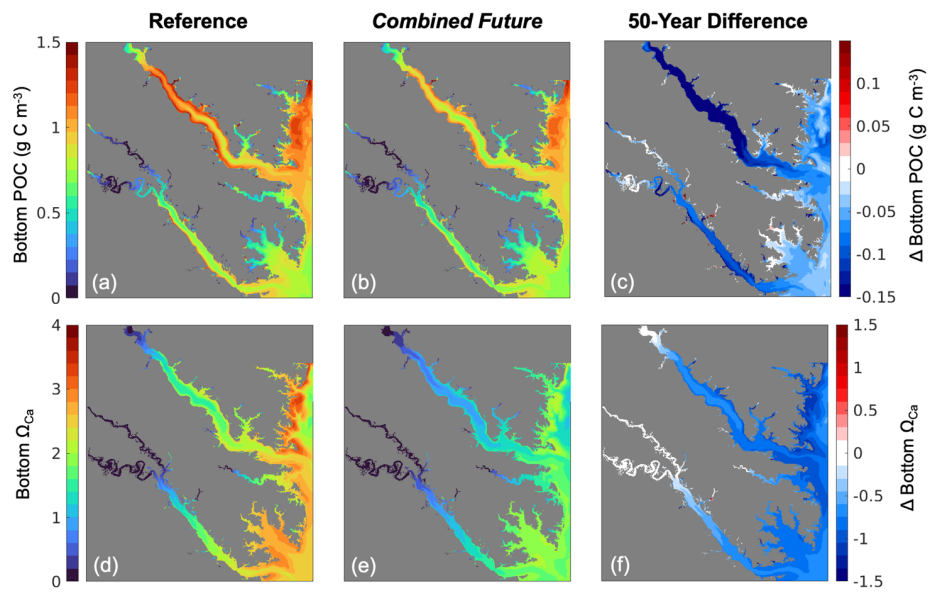


Figure 6. Annual mean bottom (a-c) POC and (d-f) Ω_{Ca} from (a,d) the present-day reference run, (b,e) the *Combined Future* simulation, and (c,f) the difference between (a) and (b), i.e., *Combined Future* minus reference.

Moved (insertion) [14]

Formatted: Space After: 10 pt, Line spacing: single

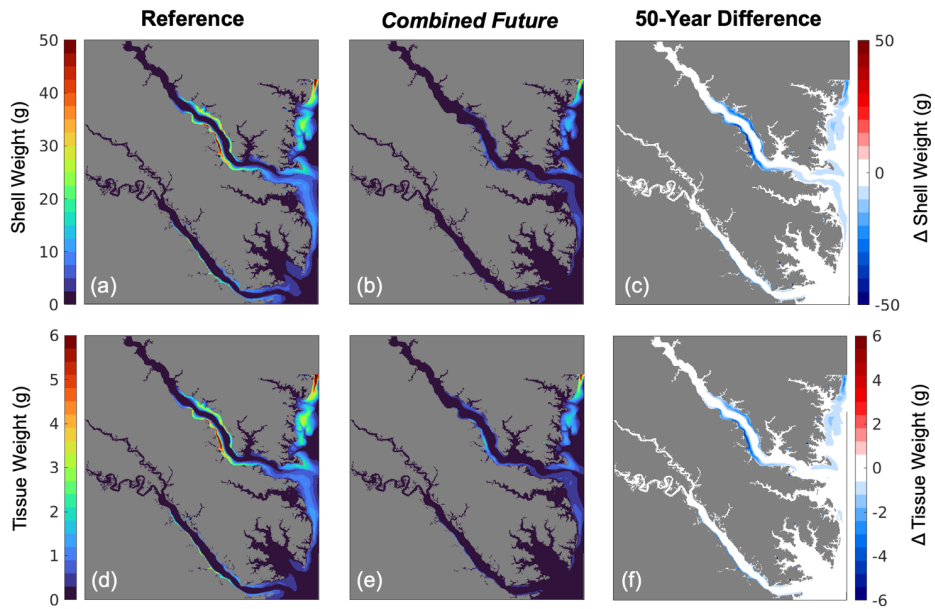
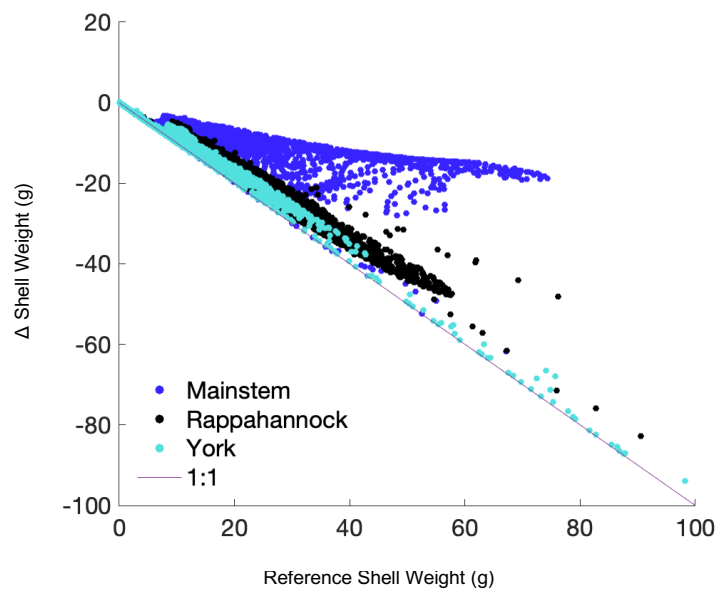


Figure 7. (a-c) Shell weight and (d-f) tissue weight at the end of the one-year simulation from (a,d) the present-day reference run, (b,e) the *Combined Future* run, and (c,f) their difference, i.e., *Combined Future* minus reference.

Deleted: ¶

1404



Formatted: Font: 10 pt, Not Bold

1405
1406
1407

Figure 8. Difference in shell weight at the end of the one-year simulation between the *Combined Future* run and the reference run, i.e., *Combined Future* minus reference, colored by region. Each point represents a grid cell where oyster growth occurs in the reference run.

Formatted: Space After: 10 pt, Line spacing: single

Deleted: 1

Formatted: English (US)

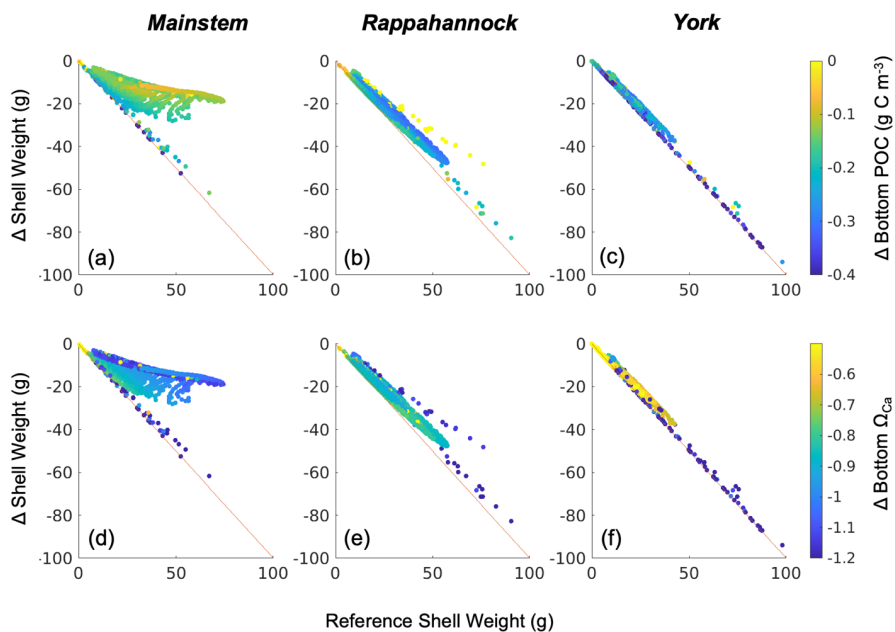
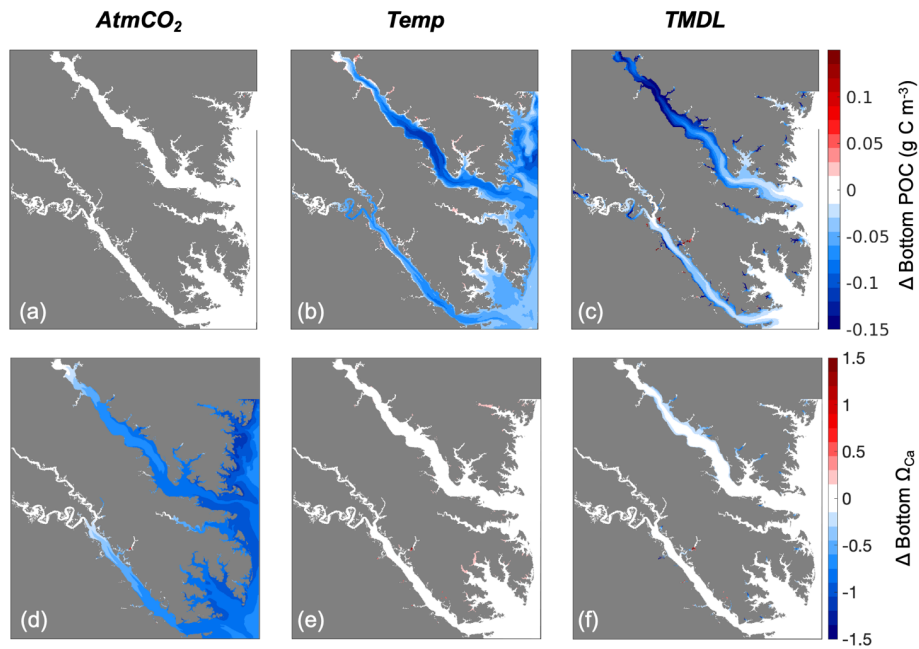


Figure 9. Difference in shell weight at the end of the one-year simulation between the *Combined Future* run and the reference run colored by (a-c) change in POC and (d-f) change in bottom Ω_{Ca} (i.e. *Combined Future* minus reference) for grid cells that support oyster growth. Results are presented for (a,d) the mainstem shoal only, (b,e) the Rappahannock River only, and (c,f) the York River only.



414 Figure 10. Differences in annual averaged (a-c) bottom POC and (d-f) bottom Ω_{Ca} (d-f) for three sensitivity experiments: (a)
 415 $AtmCO_2$, (b) Temp, and (c) TMDL. Differences represent future results minus those from the present-day reference run.

Moved (insertion) [15]

Deleted: ¶

Figure 10. Differences in annual averaged (a-c) bottom POC and (d-f) bottom Ω_{Ca} (d-f) for three sensitivity experiments: (a) $AtmCO_2$, (b) Temp, and (c) TMDL. Differences represent future results minus those from the present-day reference run. ¶

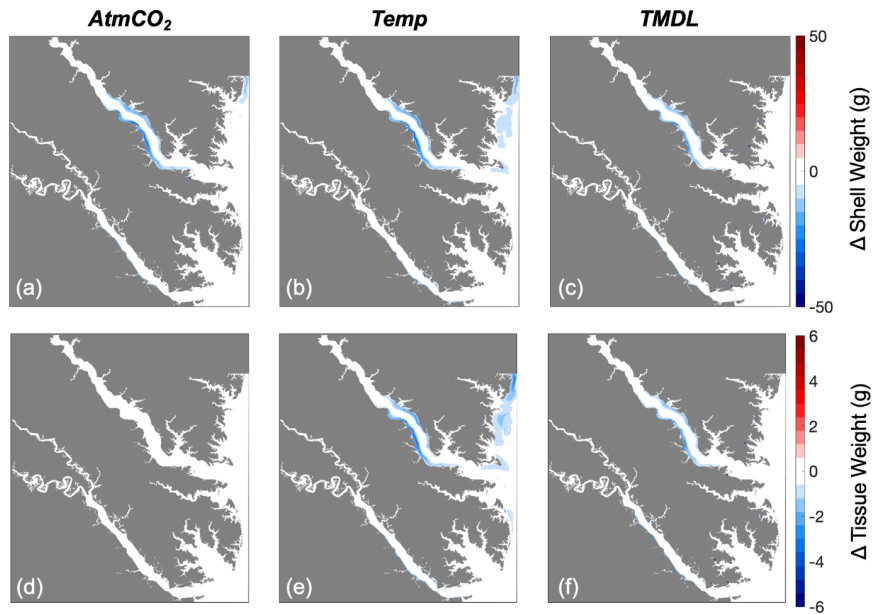


Figure 11. Differences in (a-c) shell weight and (d-f) tissue weight at the end of the one-year simulation for three sensitivity experiments: (a) AtmCO₂, (b) Temp, and (c) TMDL. Differences represent future results minus those from the present-day reference run.

Formatted: Space After: 10 pt, Line spacing: single

Formatted: English (US)

Formatted: Font: +Body (Times New Roman), English (UK)

Formatted: Left, Line spacing: single

Page 2: [1] Deleted Catherine R. Czajka 4/11/25 12:05:00 PM



Page 2: [2] Deleted Catherine R. Czajka 4/11/25 12:05:00 PM



Page 21: [3] Deleted Catherine R. Czajka 4/11/25 12:05:00 PM



Page 21: [4] Deleted Catherine R. Czajka 4/11/25 12:05:00 PM



Page 21: [5] Deleted Catherine R. Czajka 4/11/25 12:05:00 PM



Page 21: [6] Deleted Catherine R. Czajka 4/11/25 12:05:00 PM

